https://doi.org/10.5194/egusphere-2026-1428
Preprint. Discussion started: 15 April 2026

Chemical Characterization and Source Apportionment of Carbonaceous Aerosols during Post-Monsoon Biomass Burning and Diwali at an Upwind Site of Delhi

Vasu Singh[1], Dilip Ganguly[1], Jaswant Rathore[1], Lokesh Kumar Sahu[2], Ravi K. Kunchala[1], Sagnik Dey[1]

[1]Centre for Atmospheric Sciences, Indian Institute of Technology Delhi, New Delhi, India,

[2]Space and Atmospheric Sciences Division, Physical Research Laboratory, Ahmedabad, India

Corresponding Author: Vasu Singh (Vasu.Singh@cas.iitd.ac.in)

Abstract

Sonipat, located ~40 km northwest of Delhi, lies along the principal transport corridor linking post-monsoon agricultural burning regions of Punjab–Haryana with Delhi and serves as an intermediate receptor for regional pollution. We conducted intensive high time resolution measurements of composition-based $PM_{2.5}$ (non-refractory $PM_{2.5}$ plus black carbon) from 25 October to 15 November 2023 using a ToF-ACSM and an Aethalometer to characterize carbonaceous aerosol sources during the biomass-burning period. Two severe haze episodes occurred, with $PM_{2.5}$ exceeding 300 µg/m^3. Organic aerosol dominated the submicron mass (~65% of non-refractory $PM_{2.5}$), with daily mean concentrations peaking near 140 µg/m^3 during the first haze episode. Positive Matrix Factorization resolved five components including hydrocarbon-like, biomass-burning, and solid-fuel combustion organic aerosol, and two oxygenated fractions representing semi-volatile and low-volatility aged aerosol. Secondary organic aerosol accounted for ~57-60% of organic aerosol mass, with low-volatility oxygenated organic aerosol reaching 42.8 µg/m^3 during peak haze, indicating substantial regional aging and accumulation. Biomass-derived black carbon contributed ~78% of total black carbon (mean 10.9 µg/m^3), far exceeding fossil-fuel contributions (~3.1 µg/m^3). Trajectory and wind analyses consistently identified northwestern agricultural regions as dominant sources with minor traffic influence, indicating that extreme carbonaceous aerosol over Delhi-NCR largely forms outside the urban core through regional transport biomass and solid-fuel combustion emissions combined with sustained secondary processing, highlighting the need for coordinated airshed-scale emission reductions across the Indo-Gangetic Plain.

1. ***Introduction***

The Indo-Gangetic Plain (IGP) is widely recognized as one of the most polluted regions globally in terms of fine particulate matter ($PM_{2.5}$) loading and its associated atmospheric impacts (Dey and Di Girolamo, 2010; Ganguly et al., 2009; Ghude et al., 2016). This region is densely populated and a rapidly developing airshed is influenced by a complex mixture of emission sources, including vehicular traffic, industrial activities, residential biofuel consumption, and seasonal agricultural residue burning (Biswal et al., 2023; Ganguly et al., 2009). Within the IGP, the Delhi-National Capital Region (Delhi-NCR) frequently experiences severe haze episodes, particularly during the post-monsoon and winter seasons (Gani et al., 2019), when $PM_{2.5}$ concentrations can exceed World Health Organization (WHO) guidelines by an order of magnitude or more (Rathore et al., 2025). These extreme pollution episodes have profound public health consequences. Air pollution in India has been linked to 1.67 million premature deaths in 2019, with approximately 1 million deaths attributed specifically to ambient $PM_{2.5}$ exposure (Pandey et al., 2021). Given its significance in critical scientific and policy priority, it is necessary to understand the sources and processes that drive these episodes over the study region.

Post-monsoon haze events over northern India are strongly influenced by extensive agricultural residue burning in the northwestern IGP, particularly across Punjab and Haryana, and are further reinforced by unfavorable meteorological conditions (Sarkar et al., 2018). Cold and dry northwesterly winds coincide with the post-harvest agricultural cycle, transporting biomass-burning emissions toward Delhi-NCR. At the same time, shallow planetary boundary layers (PBLs), weak ventilation, and stagnant conditions limit dispersion and enhance pollutant accumulation near the surface (Nair et al., 2007). Although the dominant drivers of these episodes are broadly understood, robust quantification of individual source contributions and their evolution during regional transport remains limited. This limitation is particularly pronounced at upwind locations outside the urban core, where transported air mass begins to interact with local emissions and undergoes complex chemical processing before reaching megacity environments (Lalchandani et al., 2022).

https://doi.org/10.5194/egusphere-2026-1428
Preprint. Discussion started: 15 April 2026

Reliable source apportionment is essential for designing effective mitigation strategies. Policy frameworks such as the Graded Response Action Plan (GRAP) depend on accurate identification of dominant sources, yet separating regional background pollution from episodic enhancements associated with biomass burning and festival-related emissions remains challenging (Ghude et al., 2024; Pant et al., 2016; Yadav et al., 2022). During the post-monsoon period, intense agricultural burning and Diwali firework emissions can both elevate $PM_{2.5}$ concentrations (Satish et al., 2017; Thamban et al., 2019). Their chemical signatures often overlap with those from domestic cooking and heating, complicating attribution (Tobler et al., 2020). Distinguishing these contributions is critical because the relative importance of primary versus secondary sources has direct implications for control strategies. For example, if secondary aerosol formation dominates, mitigation efforts targeting only primary emissions may be insufficient to significantly reduce peak pollution levels.

Most of the previous studies on source apportionment in the region have relied on filter-based receptor modelling, which typically provides 24-hour averaged chemical composition (Jain et al., 2019; Sharma et al., 2016). While such approaches yield valuable information on bulk aerosol composition, they lack the temporal resolution required to capture rapid chemical transformations and short-lived pollution peaks. Intense but transient emissions from firework displays, moving fire plumes, or episodic industrial activities can be substantially smoothed in daily averages. Moreover, measurements conducted within dense urban environments are often dominated by local traffic and industrial emissions, which can mask the signatures of regionally transported aerosols (Bhandari et al., 2020; Guttikunda and Calori, 2013; Singh et al., 2021). These limitations highlight the need for high-time-resolution measurements at strategically located receptor sites to isolate regional contributions.

Advances in online aerosol instrumentation provide new opportunities to overcome these challenges. Instruments such as the Time-of-Flight Aerosol Chemical Speciation Monitor (ToF-ACSM) enable continuous, high-time-resolution measurements of non-refractory aerosol species and can resolve rapid changes in chemical composition associated with evolving atmospheric processes (Fröhlich et al., 2013; Ng et al., 2011). When combined with Positive

Matrix Factorization (PMF), these datasets can be decomposed into sources related to organic aerosol factors without requiring a priori source profiles (Canonaco et al., 2013). This approach has been widely applied across complex source regions within the IGP to differentiate fresh biomass burning organic aerosol (BBOA) from more aged, oxygenated organic aerosol (OOA), thereby providing deeper insight into aerosol evolution beyond bulk chemical characterization (Lakra et al., 2024; Shukla et al., 2025). Recent studies have identified solid-fuel combustion organic aerosol (SFCOA) and oxygenated organic aerosol (OOA) as major contributors to organic mass in Delhi (Lalchandani et al., 2022) and Faridabad (Tobler et al., 2020). However, most such investigations have focused on urban receptor sites, leaving the transformation and mixing processes of carbonaceous aerosols during regional transport poorly constrained .

In this context, Sonipat, located northwest of Delhi along the dominant pollution transport corridor from Punjab and Haryana, represents a strategically important upwind receptor site. Air masses arriving at this location intercept regional biomass-burning plumes before they are substantially mixed with strong local emissions from the Delhi metropolitan area (Singh et al., 2023). Recent chemical characterization at this site during the post-monsoon period indicated that carbonaceous aerosols accounted for nearly 80% of composition-based $PM_{2.5}$ mass, with relatively minor contributions from secondary inorganic species (Rathore et al., 2025). This composition differs from haze episodes in other regions such as the North China Plain, where secondary sulfate and nitrate often dominate. Analysis of satellite-derived vegetation indices and fire counts data reveals increasing agricultural burning activity in source regions upwind of Sonipat (Jethva et al., 2019), supporting the observations of enhanced aged organic aerosol at this site (Rathore et al., 2025). Although earlier work characterized bulk aerosol chemistry and highlighted the importance of biomass burning emissions, substantial variability during the Diwali festival and post-rainfall periods suggests the presence of multiple temporally varying sources that cannot be resolved through bulk analysis alone. Periods of relatively clean air following rainfall, followed by rapid pollution buildup during Diwali, provide a natural experiment for examining source dynamics under changing meteorological and emission conditions.

https://doi.org/10.5194/egusphere-2026-1428
Preprint. Discussion started: 15 April 2026

Based on the research literature, there are several questions yet to be addressed for better understanding the role of the source contributions and evaluating the effectiveness of emission control strategies. I have tried to answer some of those questions in this manuscript as follow:

1) What are the relative contributions of transported biomass burning emissions and local sources such as traffic and industry emissions during peak haze conditions at this upwind location?

2) To what extent does primary organic aerosol dominate over secondary formation under conditions of weak photochemistry and limited inorganic precursor availability?

Addressing these questions is essential for evaluating the effectiveness of emission control strategies. A detailed, high-time-resolution source apportionment is therefore required to disentangle the contributions of individual sources and to assess the balance between primary and secondary carbonaceous aerosols during regional transport into Delhi.

In this study, we present a comprehensive source apportionment of $PM_{2.5}$ at the upwind Sonipat site during the post-monsoon biomass-burning and Diwali period, building upon our earlier chemical characterization study (Rathore et al., 2025). Using high-time-resolution ToF-ACSM and Aethalometer measurements in conjunction with receptor modeling and trajectory analysis, we resolve carbonaceous aerosol into source-specific components and examine their temporal variability in relation to meteorology and independent tracers. The primary objectives are to (i) identify and quantify major organic aerosol sources during haze and non-haze conditions, (ii) assess the relative contributions of transported biomass burning emissions, local traffic, industrial sources, and secondary formation, and (iii) contrast source dynamics between prolonged biomass-burning episodes and the transient Diwali event. This work provides one of the first high-resolution $PM_{2.5}$ source apportionment analyses at a strategically located upwind gateway to Delhi and offers new constraints on regional transport processes and source contributions relevant for air quality management across the Delhi-NCR and the broader Indo-Gangetic Plain.

2. Materials and Methods

2.1. Study Site Description

Measurements for this study were conducted at the Center for Atmospheric Sciences–Atmospheric Observatory (CAS-AO) located on the IIT Delhi Sonipat campus (28.95°N, 77.10°E; 228 m above mean sea level). The observatory is situated approximately 14 km upwind of the Delhi border in the state of Haryana and lies within the National Capital Region (NCR). The site is positioned in a semi-urban environment within the Rajiv Gandhi Education City and is surrounded by a heterogeneous land-use matrix comprising academic institutions, agricultural fields, small-scale industrial activities, and major national highways. This setting makes the site well suited for investigating the combined influence of regional and local emissions. The geographic location of the observational site, and an image of the installed ToF-ACSM are presented in Figure1.

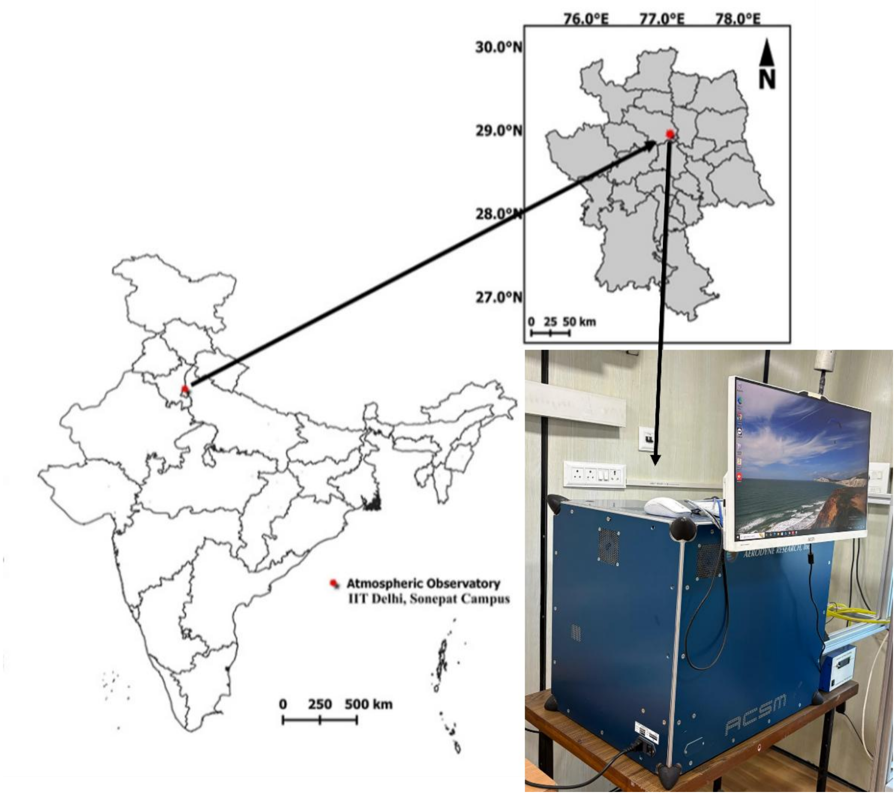

https://doi.org/10.5194/egusphere-2026-1428
Preprint. Discussion started: 15 April 2026

Figure 1: *Location map of the study site (marked by a star symbol) and a photograph of the installed ToF ACSM.*

The regional climate is characterized by hot summers, a humid monsoon season, and cold winters, broadly similar to prevailing meteorological conditions over Delhi. During the pre-monsoon (March–May) and monsoon (June–September) seasons, the site is frequently affected by dust transport from Thar Desert. In contrast, the post monsoon (October–November) and winter (December–February) seasons are characterized by frequent haze and smog episodes that substantially degrade visibility and air quality. During the post-monsoon period, northwesterly winds often transport polluted air masses from the agricultural regions of Punjab and Haryana, where large-scale crop-residue burning occurs(). In addition to these regional influences, the site is also affected by local vehicular emissions, nearby industrial activities, and biomass-burning sources. Owing to its proximity to Delhi and similarity in meteorological conditions, the site provides a representative location for examining aerosol processes relevant to the Delhi-NCR region. Additional details regarding the site characteristics, measurement, and long-term observations are provided in Rathore et al. (2025).

2.2. Instrumentation and Measurements

This study utilizes measurements conducted between 25 October 2023 to 16 November 2023 at the CAS-AO site using multiple state-of-the-art instruments. Non-refractory submicron particulate matter (NR-$PM_{2.5}$) was measured using a Time-of-Flight Aerosol Chemical Speciation Monitor (ToF-ACSM; Aerodyne Research, Inc., Billerica, Massachusetts, USA) equipped with a $PM_{2.5}$ aerodynamic lens and a capture vaporizer. The instrument was housed in a temperature-controlled room on the top floor(18m above ground) of I-TECH building at the observatory to ensure stable operating conditions. The ToF-ACSM measures the mass concentration of non-refractory aerosol species that flash vaporize at temperature above ~600 °C. Vaporized species are ionized using 70eV electron-impact ionization, and the resulting ions are analyzed by a time-of-flight mass spectrometer (Fröhlich et al., 2013; Nault et al., 2023). The inlet system was specifically set up to enable the ToF-ACSM and the SMPS to run alongside each other at the same time, sharing a common sampling line. The instrument is equipped with a 3.05m copper tube and a $PM_{2.5}$ cyclone at beginning of the inlet ensuring only fine particles (smaller than 2.5 µm) are analyzed from outside the window. The sampling line also has water trap and a Nafion membrane diffusion dryer(Perma Pure MD) to remove moisture from the aerosol sample. The system operates at a total flow rate of 2.5 L min^{-1}. This flow is split between the connected instruments- the SMPS draws 1 L min^{-1}, the ToF-ACSM pulls approximately 0.1 L min^{-1}, and the leftover 1.4 L min^{-1} is handled by an in-line flow controller to maintain the overall balance. During the entire sampling period, the vaporizer was maintained at a temperature below 600°C(approximately 525–530°C). For the data analysis, a composition-dependent collection efficiency (CDCE) value of 1 was applied to the capture vaporizer system, in line with the approach recommended by (Hu et al., 2018). The instrument provides high-time-resolution measurements of organic aerosol, sulfate, nitrate, ammonium, and chloride with a 40-s time resolution, with 20 seconds of each cycle dedicated to background or filter sampling. Standard operating procedures, including calibrations, air-beam corrections, application of fragmentation tables, and uncertainty estimation, were performed using the TOFWARE 4.4.1 data analysis package prior to further processing.

Black carbon (BC) mass concentrations were measured using a seven–wavelength Aethalometer (model AE31; Magee Scientific, Berkeley, California, USA), which provides wavelength-dependent aerosol light absorption coefficients. The AE31 Aethalometer had its own dedicated sampling arrangement, independent of the ToF-ACSM inlet AE31 sampled the ambient air at the rate of 2 L min^{-1} through a 2.5m long conductive tube, with $PM_{2.5}$ cyclone. The vertical structure of the lower atmosphere, including atmospheric boundary layer (ABL) height and depolarization ratios, was monitored using a Vaisala CL61 ceilometer. Meteorological parameters, including temperature, relative humidity, wind speed, and wind direction, were obtained from an automatic weather station (AWS) installed at the site. Detailed descriptions of all the instrument configuration, inlet setup, calibration protocols, and data acquisition procedures are discussed in Rathore et al. (2025).

2.3. Source-apportionment Techniques

https://doi.org/10.5194/egusphere-2026-1428
Preprint. Discussion started: 15 April 2026

Receptor-based source apportionment techniques were applied to identify and quantify major sources contributing to submicron aerosol mass at the study site. These methods resolve the observed aerosol composition into a limited number of source-related factors based on characteristic temporal and chemical signatures.

2.3.1. **Positive Matrix Factorization (PMF)**

Positive Matrix Factorization (PMF) was applied to the organic aerosol mass spectral dataset to apportion sources of submicron particulate matter. PMF is a multivariate receptor-modeling technique that decomposes the observed data matrix ***X*** into a factor contribution matrix ***G*** and a factor profile matrix ***F***, along with a residual matrix ***E***, such that:

$$\boldsymbol{X} = \boldsymbol{G}.\boldsymbol{F} + \boldsymbol{E}$$

The optimal solution is obtained by minimizing the objective function:

$$Q = \sum_{i=1}^{n}\sum_{j=1}^{m}\left(\frac{e_{ij}}{\sigma_{ij}}\right)^{2}$$

where e_{ij} represents residuals and σ_{ij} denotes measurement uncertainties. This weighting scheme reduces the influence of variables with higher uncertainty on the solution (Paatero and Tapper, 1994). PMF has been widely used in aerosol mass spectrometry studies and is particularly well suited for resolving organic aerosol sources from high-time-resolution datasets (Ulbrich et al., 2009).

PMF analysis was performed using the Source Finder (SoFi, version 8) interface (Datalystica Ltd.) implemented in Igor Pro. SoFi provides an interactive framework that enables evaluation of rotational ambiguity through FPEAK exploration, as well as displacement and bootstrap analyses to assess solution stability. The tool also allows direct comparison of factor profiles with reference spectra from previous studies (Canonaco et al., 2021, 2013). The input data consisted of organic mass spectra from the TOF-ACSM, preprocessed using standard

TOFWARE routines, including air beam correction, application of fragmentation tables, and uncertainty estimation. Factor identification was guided by time series behavior, diurnal patterns, correlations with external tracers, and comparison with established reference spectra.

2.3.2 Aethalometer-Based Source Apportionment of Black Carbon

The multi-wavelength AE31 Aethalometer data were used to apportion black carbon sources using the Aethalometer Model proposed by Sandradewi et al. (2008). This model exploits the wavelength dependence of aerosol light absorption to differentiate between fossil-fuel combustion and biomass or wood combustion. Absorption coefficients at 470 nm and 950 nm were used, as this wavelength pair provides strong contrast between traffic-related and biomass-burning aerosols (Sandradewi et al., 2008; Zotter et al., 2017).

$$b_{abs}(\lambda) = b_{abs,ff}(\lambda) + b_{abs,bb}(\lambda)$$

It is assumed that the total absorption coefficient at a certain wavelength is the sum of contributions from fossil fuel (ff) and wood burning (bb) sources. The spectral dependence of absorption follows a power-law relationship:

$$b_{abs}(\lambda) \propto \lambda^{-\alpha}$$

where **α** is the Ångström exponent for absorption. We adopted fixed **α** values of 1.0 for fossil fuel combustion and 2.0 for biomass burning (Figure S9), consistent with values reported in previous studies conducted in Delhi-NCR and other urban regions of northern India (Tobler et al., 2020). By solving the coupled equations described in Sandradewi et al. (2008), fractional contributions of biomass-burning black carbon (eBC_{bb}) and fossil-fuel black carbon (eBC_{ff}) were determined. Data screening and quality control followed procedures outlined by Segura et al. (2014). The analysis methodology followed the approaches outlined by Harrison et al. (2013); Kumar et al. (2020) and Titos et al. (2017). Following Petzold et al. 2013, the term equivalent black carbon (eBC) is used to denote absorption-derived BC.

This method has been widely applied in Delhi and across the IGP to quantify contributions from vehicular emissions and biomass combustion, particularly during winter and the post-

https://doi.org/10.5194/egusphere-2026-1428
Preprint. Discussion started: 15 April 2026

monsoon periods (Bikkina et al., 2019; Dumka et al., 2018). Despite inherent assumptions regarding fixed spectral exponents, the method provides a robust and widely accepted framework for source attribution of black carbon in complex urban and semi-urban environments.

2.4. Trajectory and Wind Based Source Analysis

To identify potential source regions influencing the receptor site, concentration-weighted trajectory (CWT) analysis was conducted using the ZeFir toolkit by Petit et al. (2017). Five-day air mass back trajectories were computed at hourly time resolution using the Hybrid Single-Particle Lagrangian Integrated Trajectory (Hysplit v4.1) model (Draxler et al., 2018; Stein et al., 2015), driven by Global Data Assimilation System (GDAS) meteorological fields at 1° × 1° a spatial resolution. These trajectories combined with time series of organic aerosol factors to compute CWT fields according to:

$$CWT_{ij} = \frac{1}{\tau_{ij}} \sum_{k=1}^{N} C_k \tau_{ijk}$$

where, C_k is the measured concentration associated with trajectory k, and τ_{ijk} is the residence time of trajectory k in the grid cell i j. This approach identifies geographic regions associated with elevated concentrations at the receptor site. Organic aerosol factor time series were averaged to 3-hour intervals to match trajectory resolution.

To examine the relationship between pollutant concentrations and local meteorology, Non-Parametric Wind Regression (NWR) analysis was performed following (Henry et al., 2009). NWR applies Gaussian kernel smoothing to estimate pollutant concentrations as a continuous function of wind speed and direction, enabling separation of local and transported sources. Pollution-rose analyses were generated by combining wind direction frequency with concentration data to identify dominant source sectors. These complementary methods provide a comprehensive assessment of local and regional source influences on observed aerosol composition.

3. Results and Discussions

For consistency with our earlier chemical characterization study (Rathore et al., 2025), we partition the measurement period into four phases representing distinct emission–meteorology regimes: a pre-haze non-haze period (NH1; 25 October–1 November), a prolonged biomass-burning–dominated haze episode (H1; 1–10 November), a rain-influenced non-haze period (NH2; 10–12 November), and a second haze episode coincident with Diwali emissions (H2; 12–15 November). Rathore et al. (2025) demonstrated that bulk $PM_{2.5}$ during these phases is dominated by carbonaceous aerosols at Sonipat, indicating that this upwind site frequently experiences severe particulate loading even before air masses reach the Delhi urban core. Here, we extend that framework by resolving source-specific contributions to carbonaceous PM (organic aerosol and black carbon) and by examining how primary emissions, secondary processing, and meteorology jointly control the timing, magnitude, and composition of haze and non-haze conditions along the northwest transport corridor into Delhi-NCR. This approach is particularly relevant for mitigation because it distinguishes periods dominated by direct combustion emissions from periods where a large fraction of the mass resides in aged, oxygenated material, implying different leverage points for control strategies.

3.1. Identification and Interpretation of OA Factors

The PMF analysis applied to the ToF-ACSM organic mass spectra resolved five distinct factors: hydrocarbon-like organic aerosol (HOA), biomass-burning organic aerosol (BBOA), solid-fuel combustion organic aerosol (SFCOA), semi-volatile oxygenated organic aerosol (SVOOA), and low-volatile oxygenated organic aerosol (LVOOA), providing a physically interpretable separation between primary organic aerosol (POA) and secondary organic aerosol (SOA) (Figure 2a). The corresponding factor mass spectra and elemental ratios are shown in Figure 2a and summarized in Table S1 (Supporting Information), while bulk C-$PM_{2.5}$ (composition-based $PM_{2.5}$ = NR-$PM_{2.5}$ + BC) and OA-factor contributions are shown in Figure 2b. The emergence of two oxygenated factors alongside multiple combustion-related factors is consistent with a receptor site that intercepts both fresh regional plumes and their progressively aged products. This structure is mechanistically meaningful for the IGP post-monsoon period because haze evolution often reflects not a single source type, but the superposition of transported combustion emissions and subsequent oxidation/partitioning under stagnant boundary-layer conditions.

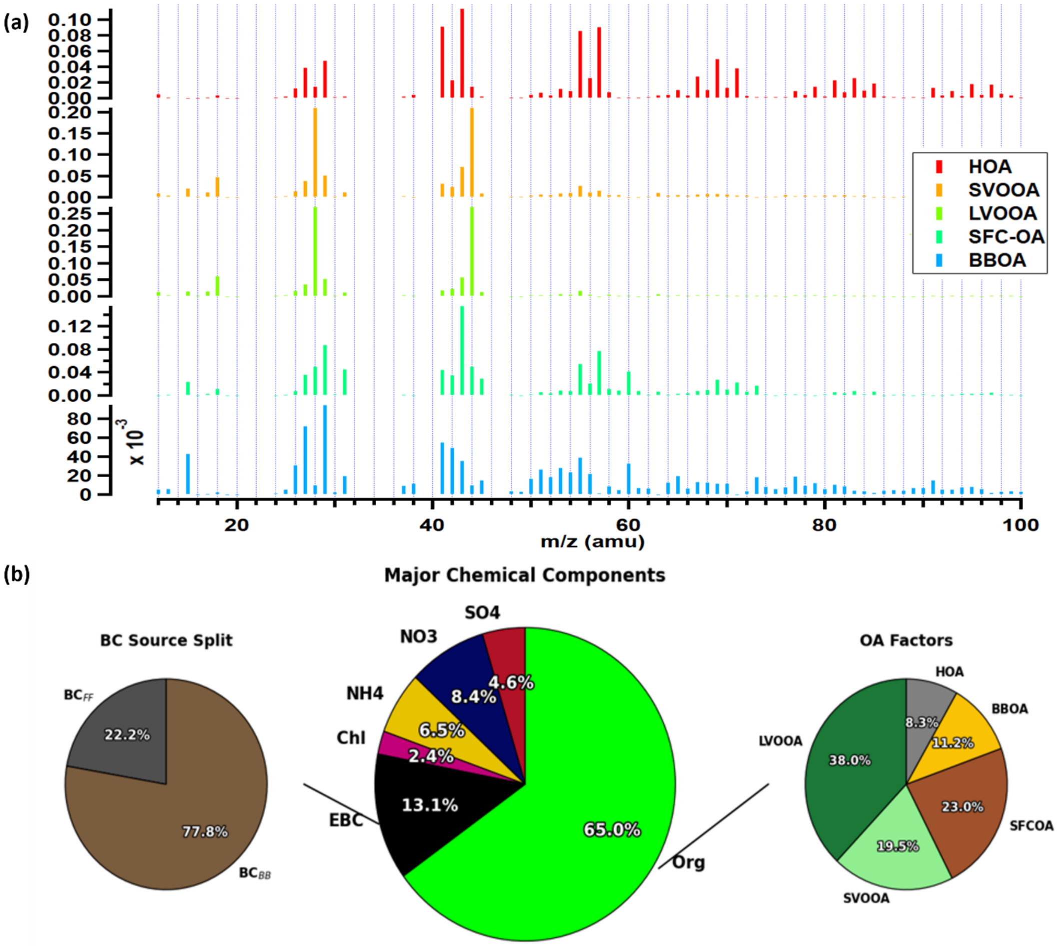

***Figure 2**: a) Mass spectra of the OA factors (HOA, SVOOA, LVOOA, SFCOA and BBOA) resolved by PMF and, b) Species contribution to C-PM$_{2.5}$ (NH_4^+, SO_4^{2-}, NO_3^-, Org, $Cl^-$and BC) (center pie*

https://doi.org/10.5194/egusphere-2026-1428
Preprint. Discussion started: 15 April 2026

chart), Relative contribution of OA factors to total OA (right pie chart) and Relative contribution of BC factors(left pie chart).

3.1.1. Primary OA Factors (HOA, BBOA, SFCOA)

HOA is characterized by prominent aliphatic hydrocarbon fragments at m/z 41, 43, 55, and 57 and low oxygenation (O:C = 0.10; Table S1 in Supporting Information), consistent with fresh traffic-related emissions. Although the five-factor solution was obtained using an unconstrained PMF framework, we constrained the HOA profile to reduce the mixing between HOA and SFCOA, which can be substantial in environments influenced by both traffic and solid-fuel combustion (Tobler et al., 2020). Specifically, we used the HOA reference profile (Canonaco et al., 2013; Crippa et al., 2013) with a randomized a-value between 0 and 0.5 to allow limited profile flexibility while stabilizing the HOA/SFCOA separation. This choice is important at Sonipat because traffic emissions are present but do not dominate the regional plume, and without this constraint, PMF can allocate part of the combustion-related hydrocarbon signal to HOA, artificially inflating traffic contributions and obscuring the relative importance of solid-fuel and biomass burning sources that are more actionable from an airshed-management perspective during post-monsoon haze.

BBOA exhibits enhanced signals at levoglucosan-related fragments m/z 60 and 73, characteristic of biomass-burning emissions(Figure 2a), and shows low oxygenation (O:C = 0.09; Table S1 in Supporting Information), indicative of fresh crop-residue burning and agricultural smoke. BBOA was a major dominant contributor during the post-monsoon haze over this site as reported in the Rathore et al. (2025). The relatively low O:C for BBOA (slightly lower than HOA) should not be interpreted as a physical inversion of oxidation state. Capture vaporizer fragmentation in ACSM-type instruments is known to underestimate O:C for certain primary and multifunctional OA by ~20-46%, compressing expected separations among primary factors (Canagaratna et al., 2015). In addition, the f44-f60 triangle shown previously (see Figure 8 of Rathore et al. (2025)) indicates strong dominance of fresh BBOA during the biomass-burning period, consistent with the interception of relatively unprocessed smoke at this peri-urban receptor in the IGP. From a process standpoint, the identification of a strong fresh biomass-burning factor at Sonipat indicates that a substantial fraction of primary carbonaceous aerosol can reach this upwind receptor directly, without requiring significant atmospheric processing within Delhi. This finding highlights that peak PM levels across the wider NCR are strongly influenced by episodic regional open burning, and therefore cannot be effectively mitigated by city-level measures alone.

SFCOA accounts for a substantial fraction of OA (23%)(Figure 2b) and is characterized by elevated aromatic fragments (e.g., m/z 55), along with m/z 60 and m/z 73 peaks(Figure 2a) that are lower than in BBOA (Tobler et al., 2020). It also exhibits moderately elevated oxygenation O:C = 0.21(Table S1 in Supporting Information), suggesting a mixture of residential and small-scale industrial solid fuel combustion. SFCOA is moderately oxygenated (O:C = 0.21; Table S1 in Supporting Information), which is consistent with a mixed source class combining residential solid-fuel use (e.g., wood/dung/crop burning residues) and small-scale industrial combustion typical of peri-urban northern India. The partial overlap in tracer ions between BBOA and SFCOA is expected, but the resolved profiles and their temporal behavior (Section 3.1.6) suggest that the two factors capture distinct emission mixtures and, potentially, distinct combustion practices and fuel types. This distinction is valuable for mitigation because agricultural open burning and household/industrial solid-fuel combustion respond to different regulatory and socio-economic interventions. The prominence of SFCOA at an upwind NCR site further indicates that strategies focused exclusively on urban traffic controls will have limited impact on the dominant carbonaceous components during post-monsoon haze periods when the regional plume is the controlling influence.

1.1.2. Secondary OA Factors (SVOOA, LVOOA)

SVOOA and LVOOA components separated primarily by oxidation state and volatility (Guo et al., 2020), together constitute approximately 57.5% of the total OA mass (Figure 2b). The higher contribution of SVOOA and LVOOA, indicates that secondary processing is a dominant contributor to carbonaceous aerosol even at this upwind receptor. LVOOA is the largest single OA component (38%) and is characterized by strong m/z 44 (CO_2^+) and high oxygenation (O:C = 0.91; Table S1), indicative of highly aged, regionally transported aerosol(Figure 2a). The stronger

https://doi.org/10.5194/egusphere-2026-1428
Preprint. Discussion started: 15 April 2026

m/z 44 signal in SOA relative to POA is associated with thermal decomposition of highly oxygenated organic acids (Ng et al., 2010). LVOOA is also distinguished from SVOOA by a lower f43/f44 ratio (0.22 for LVOOA versus 0.33 for SVOOA), consistent with more extensive oxidation and functionalization. SVOOA is also oxygenated but comparatively less aged (O:C = 0.72; Table S1), consistent with a fresher SOA fraction formed through rapid oxidation and/or partitioning of semi-volatile products during transport. As expected, SVOOA also shows a lower O:C value of 0.72 than LVOOA, which represents a comparatively fresher secondary fraction formed through rapid oxidation of volatile organic precursors.

The persistence of a large oxygenated fraction at Sonipat is mechanistically important because it suggests that secondary mass is not merely a downwind feature of Delhi's urban atmosphere but is already established in the upwind, before mixing with the local urban emissions. This implies that reducing peak $PM_{2.5}$ concentrations during post-monsoon haze is unlikely to be achieved solely by controlling urban emissions and instead requires coordinated control of regional emission sources that supply both primary organic mass and the chemical feedstock for continued oxidation and aging. In addition, the dominance of LVOOA indicates that haze periods can be sustained by a regional aged background even when short-lived primary spikes subside, meaning that mitigation measures must address both episodic emission and the underlying transported burden that sets the baseline on which those pulses are superimposed.

3.1.3. Black carbon source apportionment and linkage to OA sources

Aethalometer based BC source apportionment reveals a pronounced dominance of biomass/wood burning related equivalent black carbon (eBC_{bb}), which accounts for approximately 77.8% of total BC, compared with fossil-fuel related black carbon (eBC_{ff}, 22.2%) (Figure 2b). This strong biomass-burning signature is consistent with the geographical setting of the Sonipat site that is along the principal post-monsoon transport pathway connecting the agricultural burning regions of Punjab and Haryana to the Delhi-NCR. In addition to open-field residue burning, widespread use of solid fuels (wood, dung, and crop residues) across peri-urban and rural northern India likely contributes to the observed biomass dominated BC. The relatively modest fossil-fuel contribution reflects the reduced influence of dense urban traffic at this

https://doi.org/10.5194/egusphere-2026-1428
Preprint. Discussion started: 15 April 2026

upwind receptor during haze episodes that are largely governed by regional smoke transport under shallow and stagnant boundary-layer conditions. The BC apportionment is also internally consistent with the behavior of the PMF resolved organic aerosol factors(Figure S1; Figure S4), which show enhanced contributions from biomass-burning and solid-fuel combustion OA during polluted periods, thereby supporting a coherent combustion-driven interpretation of the carbonaceous aerosol mixture.

In absolute terms, biomass-burning BC (eBC_{bb}) averaged 10.9 µg m^{-3} over the study period, substantially exceeding fossil-fuel BC (eBC_{ff}), which averaged 3.1 µg m^{-3}(Table S2). This pattern contrasts sharply with observations from urban Delhi, where fossil-fuel BC typically dominates during winter and post-monsoon periods. For example, Dumka et al. (2018) reported that eBCff contributed about 72% of total BC (17.6 µg m^{-3}) compared with 6.8 µg m^{-3} from biomass burning during December 2015–February 2016, while (Goel et al., 2021) found fossil-fuel BC contributions of 68.85% (7.90 µg m^{-3}) versus 31.15% (4.73 µg m^{-3}) from biomass burning during August–November 2020. In contrast, the Sonipat observations show a reversed distribution, with biomass-burning sources accounting for nearly four-fifths of total BC, reinforcing the interpretation of this location as a regional receptor for transboundary combustion emissions rather than a traffic-dominated urban environment.

Beyond source attribution, this predominance of biomass-derived BC has important implications for both air quality and regional climate. BC emitted alongside biomass-burning organic species can substantially modify aerosol optical properties, enhance light absorption, and contribute to atmospheric heating, which in turn may influence boundary-layer stability and pollutant accumulation during haze events (Sahu et al., 2012; Shiraiwa et al., 2008). Although detailed quantification of such radiative and dynamical feedback is beyond the scope of the present analysis, the strong co-variation between biomass related BC and combustion-derived OA factors indicates that emission-control strategies targeting post-monsoon biomass and solid-fuel combustion would simultaneously reduce light-absorbing carbon and the bulk organic aerosol mass that drives elevated $PM_{2.5}$ at this upwind receptor.

3.1.4. Inorganic Fraction and Implications for Haze Chemistry

Although secondary inorganic aerosols (NO_3^-, SO_4^{2-}, NH_4^+, and Cl^-) account for only ~20% of bulk $PM_{2.5}$ mass (Figure 2b), the dominance of oxygenated OA within the organic fraction implies that secondary mass growth at Sonipat is more strongly governed by organic oxidation/aging processes than by inorganic neutralization and salt formation. This secondary organic heavy character is consistent with a receptor that intercepts biomass-burning plumes and their processed products before the air mass mixes with stronger urban NO_x and ammonia emission environments that can promote substantial nitrate formation. The result is a haze chemical regime in which aged carbonaceous aerosol, rather than sulfate/nitrate, plays an outsized role in determining PM mass and optical properties at this upwind gateway to Delhi-NCR.

This contrast is important for understanding why Delhi-centric mitigation strategies that prioritize NO_x-, NH_3-, or sulfate (SO_4^{2-}) driven inorganic aerosol control may not fully address the severity of upwind haze during the post-monsoon period. At Sonipat, the dominant mass resides in carbonaceous aerosol, much of it oxygenated, implying that regional combustion controls and interventions that reduce primary carbonaceous emissions and their reactive precursors are likely to provide stronger leverage for reducing the intensity of upwind haze events that subsequently influence Delhi-NCR. At the same time, the presence of non-negligible nitrate and chloride indicates that thermodynamic partitioning and multiphase processes still contribute to the aerosol burden, particularly during cool, humid and stagnant conditions that favor condensation and heterogeneous processing, setting up conditions conducive to sustained haze for longer duration.

3.1.5. Comparison with prior OA factorization studies over Delhi and the IGP

A significant amount of work over Delhi and the wider IGP has reported the dominant role of SOA contributions, particularly LVOOA, though with strong seasonality and event dependence (Bhandari et al., 2020; Bhowmik et al., 2022; Goel et al., 2024; Lalchandani et al., 2022). For example, Shukla et al., 2021 applied PMF to ACSM measurements during summer season in Delhi and found strong LVOOA dominance, consistent with extensive photochemical aging under high insolation and oxidant availability. Wintertime and post-monsoon studies more complex coupling between primary emissions and secondary processing. Thamban et al. (2021), demonstrated that SOA enhances not only OA but also the effective mass loading of primary OA families and wintertime inorganic species (e.g., nitrate and chloride), pointing to multiphase processing and nocturnal chemistry as critical amplifiers during haze (Haslett et al., 2023; Mathai et al., 2026).

More recent urban investigations further support this framework. Lalchandani et al. (2021) resolved traffic, biomass-burning, and oxygenated OA factors over Delhi and highlighted strong coupling between biomass-burning emissions and secondary OA formation during post-monsoon and winter periods. Similarly, Reyes-Villegas et al, (2021) reported oxygenated OA dominance during polluted conditions, consistent with enhanced oxidation states reflecting regional transport and aging. Across the IGP, (Panda et al., 2025) reported substantial LVOOA during prolonged haze, reinforcing the role of sustained secondary processing under stagnant meteorological conditions. (Cash et al., 2023) emphasized that SOA formation is strongly modulated by meteorology and episodic primary emissions, producing large temporal variability in OA composition even within the same season. Within this broader context, the prominent LVOOA fraction observed at Sonipat is consistent with the regional picture of strong secondary processing, while the magnitude and timing of primary combustion enhancements (especially SFCOA/BBOA) indicate that the proximity to upwind sources and shorter aging times can shift the balance toward primary emissions during certain periods, particularly short-lived events such as Diwali.

A key added value of the Sonipat perspective is that it enables a clearer separation of regional aerosol evolution occurring prior to arrival in Delhi from the intense urban mixing and source complexity within the city. The relatively low HOA and the dominant biomass-related BC fraction indicate that the upwind plume arriving at this intermediate receptor is compositionally distinct from Delhi's urban aerosol, and that the commonly reported large HOA contributions in Delhi represent additional urban increments rather than the nature of the regional background plume. This distinction matters for air-quality planning because it implies that a large fraction of the haze burden affecting Delhi-NCR can be pre-formed outside the city, requiring coordinated regional actions rather than city-only responses.

3.1.6. Temporal Evolution of OA Factors Across Haze and non-Haze Periods

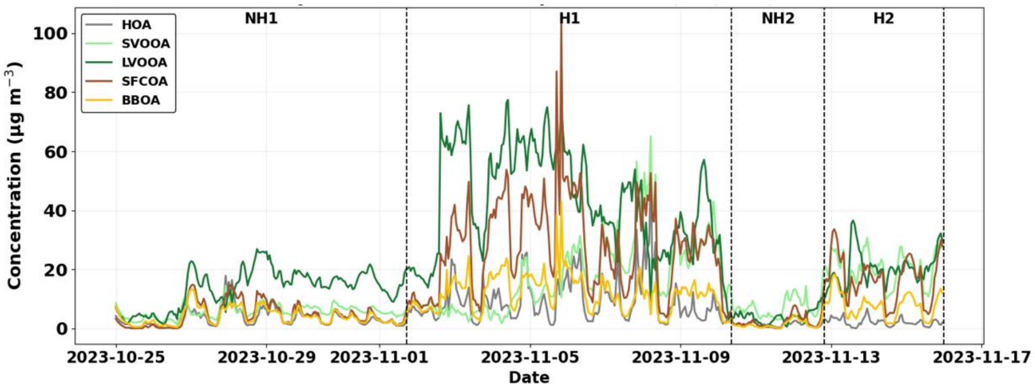

Figure 3: *Hourly time series of OA source components (µg m^{-3}) during the sampling period. Five factors were resolved via PMF: HOA, SVOOA, LVOOA, SFCOA, and BBOA. Dashed lines demarcate non-haze (NH) and haze (H) periods based on the classification criteria established by Rathore et al. (2025).*

Figure 3 shows the hourly time series of the five deconvolved OA factors during the study period. The time series reveals sharp regime shifts in both mass loading and source contributions, reflecting the combined effects of changing emissions intensity in the source regions, evolving transport pathways, and the local boundary-layer state at the receptor.

During the initial non-haze phase (NH1), OA levels were relatively modest and the background was dominated by oxygenated OA, indicating a persistent regional secondary baseline even prior to the onset of severe haze. This baseline is important because it implies that even “non-haze” conditions can carry substantial aged material, so the transition to haze represents not a clean-to-dirty switch but an amplification of an already elevated carbonaceous background. As the system transitioned into H1, all OA factors increased markedly, with especially large enhancements in SFCOA and BBOA. SFCOA increased by roughly a factor of six relative to NH conditions and exceeded 100 µg m^{-3} during 5-6 November, while BBOA increased by roughly a factor of four. The timing is consistent with intensified upwind burning activity, also reflected by elevated fire counts (Figure S12). Such concurrent enhancements of primary factors are typical of IGP haze formation when stagnant meteorology and shallow boundary layers limit dispersion and promote the accumulation of regionally transported combustion emissions (Lalchandani et al., 2022; Rathore et al., 2025). Importantly, LVOOA remained persistently elevated throughout H1, indicating that regional processing/aging continues to contribute substantial mass even during periods dominated by primary emission spikes. This sustained LVOOA suggests that multi-day accumulation and aging within the IGP transport corridor can maintain high oxygenated OA even when emission pulses fluctuate, implying that short-term episodic controls may need to be complemented by sustained reductions in regional combustion emissions to lower the baseline that supports prolonged haze.

Across the entire study period, LVOOA had the highest overall mean concentration (25.0 µg/m³), followed by SFCOA (15.1 µg/m³) and SVOOA (12.8 µg/m³) (Table S2). These concentrations are comparable to, and in some cases higher than, values reported in previous PM_1 studies from urban center Delhi, noting that our study collects the $PM_{2.5}$ that captures additional aged material at larger sizes. For example, in Old Delhi during post-monsoon, total oxygenated OA (LVOOA + SVOOA) reached 29.13 µg/m³ in PM_1 (Cash et al., 2021), whereas our $PM_{2.5}$ measurements show combined OOA (LVOOA + SVOOA) is 37.8 µg/m³, consistent with enhanced inclusion of larger, more processed material. Mean HOA (5.5 µg m^{-3}) is broadly consistent with reported HOA ranges of ~3-5 µg m^{-3} in PM_1 in Delhi (Bhandari et al., 2020; Tobler et al., 2020), reinforcing that Sonipat is not a traffic-dominated urban core receptor and that the haze burden

https://doi.org/10.5194/egusphere-2026-1428
Preprint. Discussion started: 15 April 2026

here is shaped primarily by regional combustion and subsequent aging rather than by intense local traffic increments.

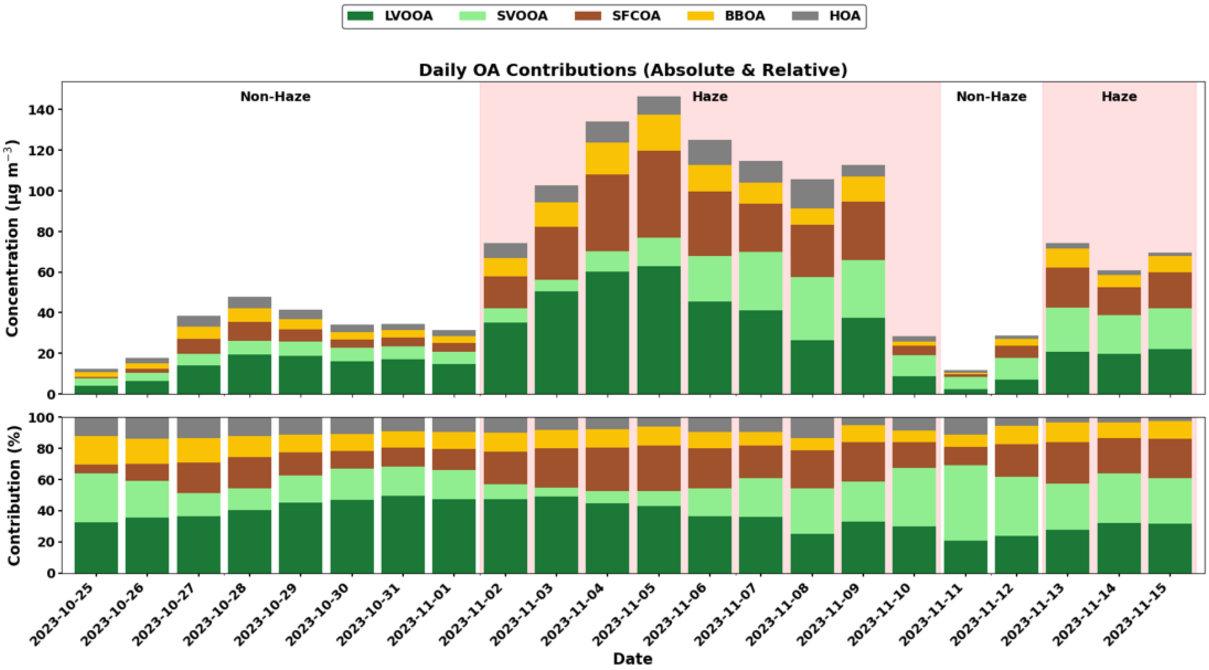

Figure 4: *Daily organic aerosol (OA) source contributions during haze and non-haze periods from 25 October 2023 to 15 November 2023. The upper panel shows absolute concentrations (μg m^{-3}) of OA factors, including low-volatility oxygenated OA (LVOOA), semi-volatile oxygenated OA (SVOOA), solid fuel combustion OA (SFCOA), biomass burning OA (BBOA), and hydrocarbon-like OA (HOA). The lower panel presents the corresponding relative contributions (%) of each OA factor to total OA. Shaded regions indicate haze periods, while unshaded regions represent non-haze conditions.*

Figure 4 presents daily absolute and fractional OA contributions. Secondary OA (SVOOA + LVOOA) remained dominant during haze periods, frequently contributing >55% of total OA, consistent with continued secondary processing under stagnant and humid conditions. At the same time, strong enhancements in SFCOA and BBOA during haze indicate that primary combustion emissions are the immediate drivers of the most intense peaks, with secondary formation contributing to large and persistent baseline on top of which primary spikes are superimposed. This structure helps reconcile two seemingly competing narratives about IGP haze: it is both combustion-driven and strongly secondary. Combustion emissions provide the mass and precursors, while stagnant meteorology and multiphase processing sustain and amplify oxygenated aerosol. Notably, during H1, LVOOA dominated early and remained persistently high, whereas during H2 the SVOOA and LVOOA contributions were more comparable, indicating differences in event character and/or processing pathways that are consistent with the shift from a prolonged regional burning episode to a shorter event with strong local/regional pulse emissions associated with Diwali.

3.1.7. Episode-wise contrasts (H1 versus H2; NH periods)

For the BC fraction, biomass burning emissions (eBC_{bb}) were the dominant contributor with an overall mean of 10.9 μg/m³, significantly outweighing the average fossil fuel fraction (eBC_{ff}), of 3.1 μg/m³(Table S2). This contrasts markedly with Delhi urban winter studies where eBC_{ff} dominated at 72% with mean eBC_{ff} of 17.6 μg/m³ versus eBC_{bb} of 6.8 μg/m³ during December 2015-February 2016 (Dumka et al., 2018) and eBC_{ff} contributed 68.85% (7.90 μg/m³) compared to eBC_{bb} at 31.15% (4.73 μg/m³) during August-November 2020 (Gupta et al., 2022). However, measurements at this upwind Sonipat site shows an opposite pattern, with wood burning accounting for approximately 78% of total BC, confirming the site's status as a regional receptor for transboundary biomass burning emissions rather than a localized traffic hotspot.

The first haze episode (H1) exhibited the highest concentrations for most factors. LVOOA reached 42.8 μg/m³ during H1 compared to 13.5 μg/m³ in the preceding non-haze period (NH1), while SFCOA increased from 4.6 μg m^{-3} (NH1) to 27.5 μg m^{-3} (H1) and BBOA from 4.0 to 11.8 μg m^{-3}(Table S2). This magnitude is exceptional when compared to reported values from Delhi-NCR and other global megacities. For instance, during severe winter haze episodes in Beijing, total OA concentrations ranged from 43.8 to 87.9 μg/m³ with SOA contributing 46-66% (Zhao et al., 2019), indicating that the aged oxygenated fraction at Sonipat during H1 approaches the lower end of total OA seen in Chinese megacity haze, despite Sonipat being a semi-urban upwind receptor.

https://doi.org/10.5194/egusphere-2026-1428
Preprint. Discussion started: 15 April 2026

This comparison demonstrates that the extreme aerosol aging and accumulation can occur over the IGP transport corridor, not only within major urban cores, and therefore regional emission reductions can yield substantial benefits by reducing the mass that is already present before the plume reaches large population centers.

Similarly, SFCOA concentrations rose dramatically from 4.6 µg/m^3 in NH1 to 27.5 µg/m^3 in H1, while BBOA increased from 4.0 µg/m^3 to 11.8 µg/m^3 (Table S2). These SFCOA levels during H1 are notably higher than typical Delhi urban winter averages, where combined SFCOA factors contributed approximately 20-35% of total OA in PM$_1$ measurements across urban Delhi and suburban Faridabad sites (Lalchandani et al., 2022; Tobler et al., 2020).

In contrast, the second haze episode (H2) showed a different SOA partitioning as SFCOA remained elevated (17.0 µg m^{-3}), but SVOOA (20.4 µg m^{-3}) became comparable to LVOOA (20.2 µg m^{-3})(Table S2). This shift points to a comparatively stronger contribution from fresh secondary formation and/or rapid partitioning processes during H2, consistent with a shorter-duration event in which newly emitted precursors and semi-volatile products can contribute strongly before being fully processed into a low-volatility fraction. Such behavior is consistent with the expectation that Diwali-period emissions can provide intense but transient injections of reactive organics and primary particles, and that the resulting aerosol may show a relatively younger oxygenated signature compared with a prolonged regional haze dominated by multi-day accumulation. The rain influenced non-haze period (NH2) was the cleanest, with LVOOA dropping to 4.1 µg m^{-3} and BBOA to 1.5 µg m^{-3}(Table S2), consistent with wet scavenging and enhanced ventilation, comparable to clean-season behavior reported for Delhi (Gani et al., 2020). The sharp reductions during NH2 also emphasize the effectiveness of meteorological cleansing in resetting the regional aerosol background, and they highlight why sustained emission reductions are needed to prevent rapid re-accumulation under the next stagnation event in H2.

During H1, eBC$_{bb}$ peaked at 14.2 µg m^{-3} while eBC$_{ff}$ averaged 3.8 µg m^{-3}(Table S2). During H2, eBC$_{bb}$ remained substantial (8.3 µg m^{-3}), while eBC$_{ff}$ decreased strongly (reported here as 0.03 µg m^{-3}), highlighting the overwhelming dominance of biomass/solid-fuel sources during that episode. These results are consistent with isotopic constraints indicating that open burning of post-harvest crop residue and wood in nearby rural regions can contribute ~42 ± 17% to severe haze in Delhi during autumn and winter (Bikkina et al., 2019); the higher biomass fraction at Sonipat is expected because of its closer proximity to upwind burning regions and weaker masking by local fossil-fuel emissions. Taken together, the episode wise contrasts indicate that the most severe events at Sonipat are driven by a combination of intensified regional combustion influence and suppressed dispersion, while the relative balance between aged and fresh oxygenated OA can shift depending on event duration, precipitation interruptions, and the presence of festival-related emission pulses. This has practical relevance because it implies that episodic interventions targeting a single source category may have limited efficacy unless they are aligned with the dominant regime as prolonged regional haze requires sustained regional combustion reductions, whereas short lived Diwali linked events may respond more to targeted restrictions and timing specific controls.

The temporal evolution of OA at Sonipat reveals pronounced shifts in both mass loading and source dominance during the transition from non-haze to haze conditions. OA constituted approximately 65% of the NR-$PM_{2.5}$ mass and exhibited multi-day accumulation episodes, with daily mean concentrations peaking near 140 µg m^{-3} during the first major haze event (H1). Under non-haze conditions, the aerosol composition was dominated by regionally aged secondary organic aerosol, particularly low-volatility oxygenated organic aerosol (LVOOA; mean ~11.2 µg m^{-3}), reflecting the persistent oxidized background characteristic of the Indo-Gangetic Plain. With the onset of haze phases (H1 and H2), there was a marked intensification of primary combustion-related factors, notably solid-fuel combustion OA (SFCOA) and biomass-burning OA (BBOA), which drove the extreme OA enhancements. This behavior is consistent with regional biomass-burning influences documented for the Delhi–NCR upwind sector (e.g., Rathore et al., 2025) and underscores the role of transported combustion emissions in modulating pollution levels at the site. Overall, the observations demonstrate that OA at Sonipat is shaped by a sustained regional oxygenated background onto which episodic influxes of primary combustion emissions are superimposed, leading to severe carbonaceous aerosol loading even before air masses mix with additional urban emissions from Delhi. These findings reinforce the necessity of airshed-scale mitigation strategies that simultaneously address regional biomass and solid-fuel combustion sources in conjunction with local urban controls.

3.2 Diurnal Variation of Carbonaceous Aerosols and effect of Meteorology

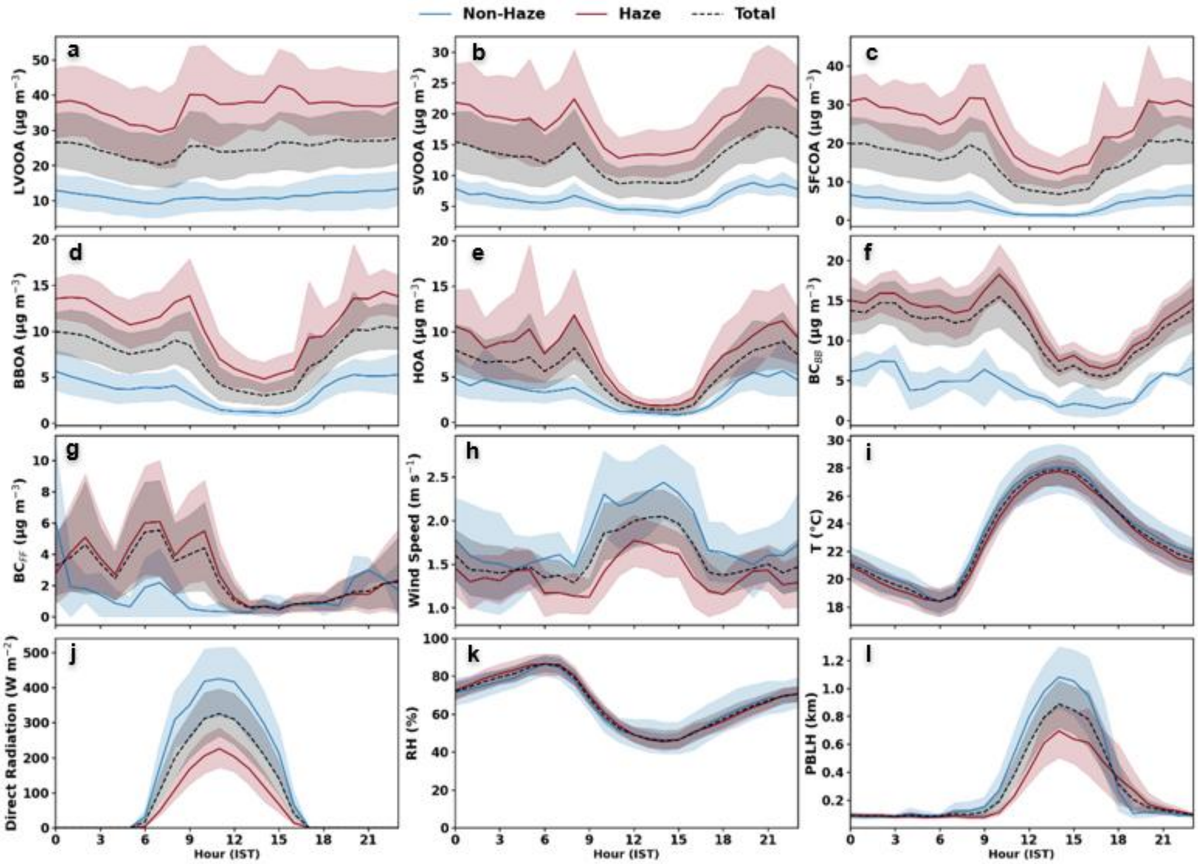

Figure 5: *Diurnal variations of PMF factors: HOA, SVOOA, LVOOA, SFCOA and BBOA; 2 resolved BC factors: eBC_{bb} and eBC_{ff} , meteorological parameters: Wind Speed, Temperature, Direct Radiation, Relative Humidity, PBLH during Haze (H1+H2), Non-Haze (NH1+ NH2) and study period (Total) from 25 October 2023 to 15 November 2023.*

Figure 5 shows mean diurnal cycles of PMF resolved OA factors (HOA, SVOOA, LVOOA, SFCOA, BBOA), the source apportioned BC components (eBCbb and eBCff), and key meteorological variables for haze (H1+H2), non-haze (NH1+NH2), and the full periods. The diurnal behavior reflects the combined influences of the variation in emission, boundary layer dynamics, and secondary formation/partitioning. The features provide a process level evidence for how daily meteorological cycling modulates both primary emission accumulation and the partitioning/aging of oxygenated aerosol components. The correlation values between different variables and their tracers can be found in supplementary material (Figure S3-S6)

3.2.1. Traffic-related factors (HOA and eBC_{ff})

The diurnal variation of both HOA and eBC_{ff} exhibit coherent diurnal variability characterized by enhanced nighttime concentrations (21:00–00:00 IST) and a secondary peak during the morning hours (06:00–09:00 IST; Figure 5e). The similarity in their temporal evolution(Figure S1) and a moderate correlation between the two species (R^2 = 0.48; Figure 5g) indicates their common origin in traffic-related emissions and with previous observations from urban and peri-urban environments (Bhandari et al., 2020; Crippa et al., 2013; Lalchandani et al., 2022). Elevated nighttime levels likely reflect increased heavy-duty vehicle activity following relaxation of daytime traffic restrictions, while the morning peak corresponds to commuter traffic. These patterns are evident under both haze and non-haze conditions; however, the amplitude of the nocturnal diurnal contrast is substantially stronger during haze episodes when shallow boundary layers suppress dilution and promote accumulation (Figure S7).

During non-haze periods, deeper daytime mixing, precipitation-driven scavenging, and reduced combustion-related activity lead to lower concentrations and a weaker diurnal contrast, in agreement with Rathore et al. (2025). Notably, the overall magnitude of HOA remains relatively modest even during severe haze, indicating that traffic emissions are not the principal driver of peak $PM_{2.5}$ at this upwind receptor. Nevertheless, localized traffic contributions can still produce short-term enhancements under nocturnal stagnation, particularly when combined with regionally transported pollution.

3.2.2. Biomass/solid-fuel factors (SFCOA, BBOA, and eBCbb)

SFCOA, BBOA, and eBCbb exhibit coherent diurnal behavior (Figure 5), with their concentrations rising from late evening (~19:00 IST), remaining elevated through the night, and declining after morning (~08:00 IST). The eBC_{bb} correlates strongly with SFCOA ($R^2 = 0.63$; Figure 5f), and BBOA exhibits an even stronger correlation with SFCOA ($R^2 = 0.95$; Figure 5d), indicating that the nocturnal enhancement reflects widespread biomass/solid-fuel combustion influences. Such nighttime peaks are consistent with residential combustion timing (cooking/heating) and with the tendency for agricultural burning and regional smoke impacts to be most pronounced under stable nighttime boundary layers (Singh et al., 2023; Tobler et al., 2020). A smaller secondary enhancement around ~08:00–10:00 IST is consistent with morning household activity and localized waste burning. As with traffic factors, haze-period boundary-layer suppression amplifies these nocturnal enhancements.

The correlated temporal variations of SFCOA, BBOA, and eBC_{bb} also imply that at Sonipat, combustion sources contributing to organic aerosol mass and light-absorbing carbon are coupled in time and likely co-located within the regional influence footprint, rather than representing independent local-only behaviors. This coupling strengthens the inference that a large fraction of the carbonaceous aerosol burden during haze is regionally coherent and thus amenable to coordinated regional interventions, including strategies aimed at reducing open burning and promoting cleaner household and small-scale industrial fuels.

3.2.3. Contrasting diurnal behavior of SVOOA and LVOOA

Similar diurnal patterns, characterized by higher nighttime and lower daytime concentrations, are observed for HOA and eBC_{ff}, during both haze and non-haze periods. However, this contrast is substantially stronger during haze conditions. The weaker diurnal contrast during non-haze periods may be associated with enhanced atmospheric mixing due to higher boundary-layer heights, precipitation-driven scavenging, and reduced combustion-related activities, as reported by Rathore et al. (2025).

SVOOA and LVOOA show clearly distinct diurnal signatures that reflect distinct formation mechanisms and atmospheric processing pathways. SVOOA shows pronounced nocturnal enhancement and covaries with particulate nitrate (NO_3^-) and chloride (Cl^-)(Figure S2), consistent with thermodynamically driven gas–particle partitioning (Zhang et al., 2021). As nighttime temperatures decrease and relative humidity increases, semi-volatile species, including inorganic nitrate and freshly formed organic oxidation products, preferentially partition to the particle phase (Lanz et al., 2007). This behavior supports the interpretation that SVOOA represents a relatively fresh SOA fraction formed through rapid oxidation of local and regional precursors followed by volatility-controlled condensation. Its diurnal variability therefore reflects both chemical production rates and equilibrium partitioning processes. In contrast, LVOOA closely tracks sulfate (SO_4^{2-}) (Figure 5a and Figure S1) and exhibits a strong correlation ($R^2 = 0.86$), indicating a regionally aged component that covaries with slower-forming secondary aerosol produced and transported over multi-day timescales. The comparatively flat diurnal profile of LVOOA further supports a transported and highly processed origin. This interpretation is consistent with previous studies over Delhi and the IGP, which attribute LVOOA to highly oxidized, carboxylic-acid-rich aerosol formed via sustained regional processing (Rathore et al., 2025; Shukla et al., 2023, 2021) and aligns with observations from other polluted megacities such as Guangzhou, where LVOOA was predominantly associated with transported aged aerosol (Guo et al., 2020). Across pollution episodes, LVOOA reaches its highest concentrations during H1, followed by H2, consistent with stronger regional accumulation during the prolonged biomass-burning haze, whereas SVOOA remains broadly comparable between H1 and H2, suggesting that once favorable thermodynamic and chemical conditions are established, the semi-volatile secondary fraction responds rapidly and approaches saturation.

The day-night contrasts summarized in Table S3 (Supporting Information) and illustrated in Figure 6 further clarify these behaviors. Transitioning from non-haze (NH1, NH2) to haze conditions (H1, H2), haze-night totals increase by approximately 3-4 times relative to NH-day baselines. For example, LVOOA rises from 12.8 μg m^{-3} (NH1 day) to 42.9 μg m^{-3} (H1 night), while SVOOA increases from 4.7 μg m^{-3} to 20.3 μg m^{-3} (H2 night). Primary combustion-related factors show similarly strong nocturnal amplification, with SFCOA increasing from 3.1 μg m^{-3} (NH1 day) to 31.2 μg m^{-3} (H1 night) and BBOA from 2.7 to 13.5 μg m^{-3}, reflecting enhanced evening combustion activity and boundary-layer contraction (Lakra et al., 2024). These findings are consistent with the post-monsoon PM_1 observations of Cash et al. (2021), where biomass-related factors (SVBBOA and SFOA) peaked under shallow nighttime boundary layers. Figure 6

https://doi.org/10.5194/egusphere-2026-1428
Preprint. Discussion started: 15 April 2026

demonstrates that haze-night composition is dominated by oxygenated secondary components (SVOOA and LVOOA, ~60%), superimposed on elevated SFCOA, BBOA, and biomass-burning black carbon (eBC_{bb}). The increase in eBC_{bb} from 13.6 to 14.8 µg m^{-3} between H1 day and night parallels the rise in SVOOA (e.g., 9.1 to 20.3 µg m^{-3} during H2), linking biomass-derived precursors to enhanced secondary formation under weakly ventilated nocturnal conditions. Comparable wintertime nocturnal enhancement of SVOOA has been reported by (Tobler et al., 2020), although the stronger nighttime increase in HOA observed here (6.6 to 12 µg m^{-3} during H1) suggests more pronounced trapping of traffic emissions under stagnation.

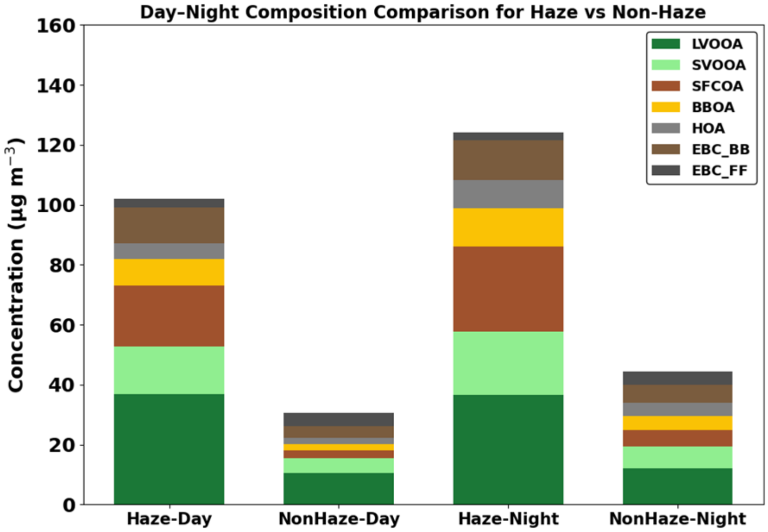

Figure 6: *Daytime and nighttime OA and eBC factors during haze and non-haze periods. Bars represent mean contributions of organic factors: HOA, SVOOA, LVOOA, SFCOA, and BBOA and EBC factors:* eBC_{ff} *and* eBC_{bb}*. Data is for the full period from 25th October 2023 to 15th November 2023.*

Meteorological conditions (Figure 5 and Figure S7) provide the physical framework underlying these compositional shifts. During haze episodes, particularly H1, planetary boundary layer heights (PBLH) remain suppressed (<500 m during daytime and <200 m at night), wind speeds are weak (often <1.5–2.0 m s^{-1}), and direct solar radiation is reduced. Elevated relative humidity (frequently 60–80%) further favors heterogeneous and multiphase processing. These

https://doi.org/10.5194/egusphere-2026-1428
Preprint. Discussion started: 15 April 2026

conditions create an effective meteorological lid that traps primary emissions (SFCOA, BBOA, HOA) while simultaneously promoting secondary mass growth and chemical aging. In contrast, non-haze periods (NH1 and NH2) are characterized by deeper daytime PBL development (often >1000 m), stronger ventilation, higher radiation, and, in NH2, rainfall-driven scavenging, leading to lower aerosol concentrations and reduced diurnal amplitude. Notably, LVOOA maintains a persistently elevated baseline during haze (~42.8 µg m^{-3} during both day and night in H1), underscoring its regional persistence. This behavior indicates that even if local emissions fluctuate, aged, oxygenated aerosols can remain elevated under stagnant conditions due to sustained regional inflow and limited ventilation. Consequently, emission reductions alone may not immediately translate into lower concentrations during strong stagnation events unless regional transport is also mitigated, as shallow boundary-layer conditions facilitate multi-day retention and recycling of aged secondary aerosol.

3.3 Primary versus Secondary Carbonaceous Aerosol Dynamics

To interpret haze growth and chemical evolution, we examine the interplay between primary and secondary components of C-$PM_{2.5}$ (Figure 7; Figure S13; Table S4-S5). Primary components (SFCOA + BBOA + HOA + eBCff + eBCbb + Cl^{-}) reflect direct combustion emissions and show strong sensitivity to activity patterns and boundary-layer dynamics, with bimodal peaks in the early morning and late evening during haze periods. As the boundary layer deepens during daytime, primary concentrations typically decrease through dilution, unless regional transport continues to supply fresh emissions. The prominence of SFCOA and BBOA in the primary budget during haze indicates that a large fraction of the peak-driving mass is combustion-derived and can respond to measures that reduce burning intensity and solid-fuel use, particularly when these measures are timed to coincide with the high-risk stagnation window.

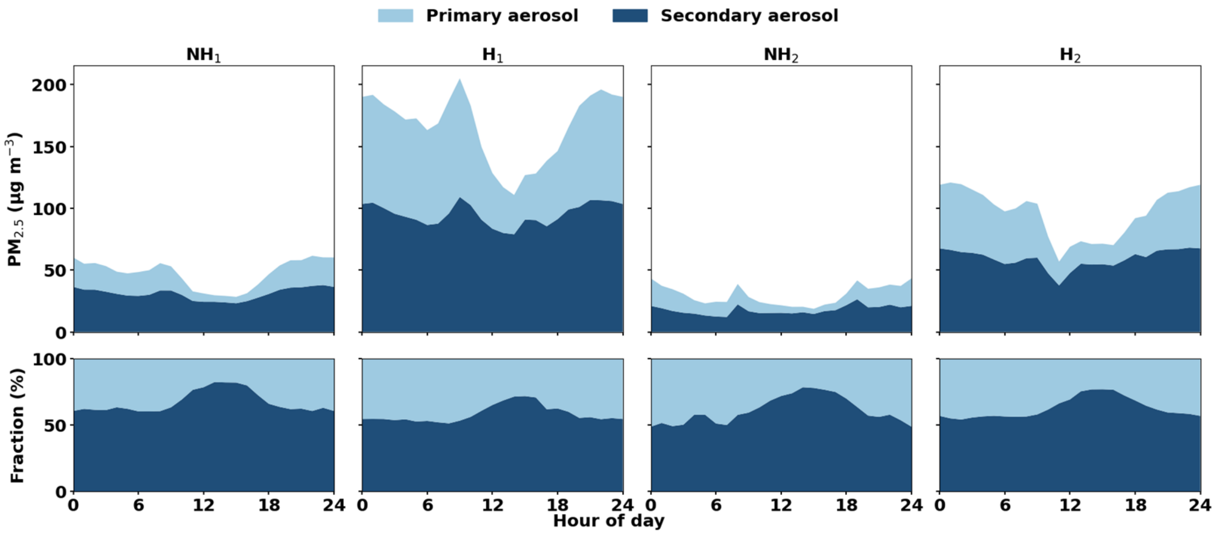

Figure 7: *Average diurnal variation of mass concentrations and mass fractions of primary and secondary C-$PM_{2.5}$ by different haze periods. Data is for the full period from 25th October 2023 to 15th November 2023.*

Secondary components (SO_4^{2-} + NO_3^- + NH_4^+ + Cl^- + LVOOA + SVOOA) form through atmospheric oxidation and multiphase processes and can remain elevated for longer periods, especially under haze-favorable conditions. During peak haze, the secondary fraction (SOA + secondary inorganics) often dominates C-$PM_{2.5}$ mass, frequently exceeding ~60%. While daytime photochemistry can contribute to secondary production, winter/post-monsoon haze in the IGP is also strongly shaped by nighttime partitioning and aqueous/multiphase reactions under high RH, allowing secondary mass to remain elevated even when direct radiation is reduced. This contributes to a positive feedback: stagnant meteorology traps primary emissions, which provide both condensational sink and reactive surfaces, promoting secondary growth and further reducing visibility. The secondary to primary ratio (Figure S13) captures this behavior: it tends to decrease during morning/evening emission peaks and increase during midday when dilution reduces primary components while secondary material persists or continues to form. In more

https://doi.org/10.5194/egusphere-2026-1428
Preprint. Discussion started: 15 April 2026

humid conditions, this ratio can remain elevated even at night, indicating continued secondary processing.

From a mitigation perspective, the sustained dominance of secondary material during the most polluted periods implies that controlling only direct primary emissions will not fully suppress peak $PM_{2.5}$ unless precursor emissions and the regional aged background are also reduced. Conversely, if secondary components dominate, mitigation efforts focused solely on primary emissions may be insufficient to reduce peak pollution levels because secondary formation and partitioning can maintain a large mass burden even when local primary increments are reduced. The Sonipat observations therefore support integrated strategies that reduce both regional combustion emissions (which supply primary mass and precursors) and the conditions that enable rapid accumulation, including targeted actions during predicted stagnation episodes when boundary-layer suppression maximizes the sensitivity of concentrations to emissions.

3.4 Biomass Burning Influence on Haze Severity

Fire counts (Figure S12) increase sharply during haze periods, indicating strong coupling between regional biomass burning and extreme pollution at Sonipat. To quantify how biomass-burning-related factors scale with pollution severity, we binned C-$PM_{2.5}$ into five concentration ranges from low (<50 µg m^{-3}) to extreme (>200 µg m^{-3}) and evaluated the fractional contributions of biomass burning (BBOA + SFCOA + eBC_{bb}), fossil fuel combustion (HOA + eBC_{ff}), secondary inorganic aerosols (SO_4^{2-} + NO_3^- + NH_4^+ + Cl^-), and secondary organic aerosol (LVOOA + SVOOA) (Figure S14). Biomass-burning contributions increase from ~21% under low pollution to ~34% under extreme pollution (>200 µg m^{-3}), indicating that intensified biomass/solid-fuel influence is a key driver of the highest PM loadings. Fossil-fuel contributions remain comparatively small (~4–10%) across all bins. SOA remains persistently large (~32–44%) across pollution levels, while secondary inorganic aerosol contributions vary less strongly.

The persistence of a large SOA fraction even at extreme pollution suggests that regional combustion emissions supply abundant precursors and aging products (including dark aging and transported oxidized OA), sustaining a substantial secondary burden (Lalchandani et al., 2022). Notably, secondary aerosol (SOA + secondary inorganics) still accounts for ~56% of C-$PM_{2.5}$ even

https://doi.org/10.5194/egusphere-2026-1428
Preprint. Discussion started: 15 April 2026

during extreme pollution, underscoring that haze severity is not solely a function of primary emissions but is strongly modulated by secondary mass growth and aging. This result has direct relevance for clean-air strategies because it implies that measures that only suppress immediate combustion activity may reduce the sharpest primary spikes but may leave a large secondary burden largely intact unless the broader regional emissions that feed secondary formation are also reduced. It also implies that actions aimed at reducing open burning can yield amplified benefits: reductions in biomass-burning emissions would simultaneously lower primary BBOA/eBC$_{bb}$ and reduce the supply of reactive organic precursors that contribute to oxygenated OA during transport.

3.5 Regional versus Local Influences: Trajectory and Wind-Based Source Diagnostics

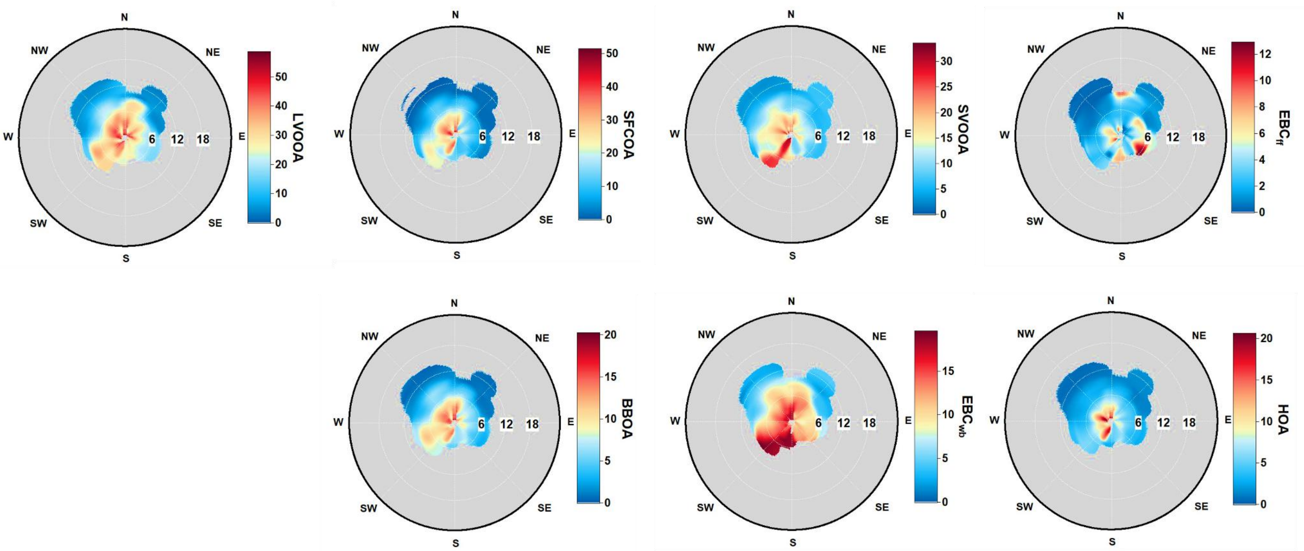

Figure 8: *Estimation of source regions using NWR approach around the site using wind speed and wind direction for organics and black carbon factors during full period from 25th October 2023 to 15th November 2023.*

To distinguish regional transport from local influences, we integrate non-parametric wind regression (NWR), pollution rose (PR) diagnostics, and concentration-weighted trajectory (CWT)

https://doi.org/10.5194/egusphere-2026-1428
Preprint. Discussion started: 15 April 2026

analysis (Figure 8; Figure S10; Figure S11). Together, these complementary methods provide a consistent framework for identifying dominant transport pathways and likely source regions, and they help interpret whether high concentrations arise predominantly from local stagnation or from coherent regional inflow.

The NWR results show that LVOOA and SVOOA exhibit strong northwest influence with peak concentrations (40-50 μg m^{-3}), consistent with regional transport along the post-monsoon corridor. PR plots (Figure S10) show that LVOOA is elevated primarily under northwest flow at moderate-to-high wind-speed percentiles (40-60+), supporting an interpretation of transported aged aerosol rather than purely local stagnation. CWT further localizes the likely source influence on the Punjab-Haryana agricultural belt, with hotspots of 15-25 μg m^{-3} for LVOOA (Figure S11). This spatial alignment with satellite-derived fire activity strengthens the inference that transported agricultural burning emissions, and their processed products contribute substantially to aged OOA at Sonipat (Gunthe et al., 2021). SVOOA shows broadly similar northwest preference, but with a wider spatial footprint in CWT, consistent with a combination of formation during transport and regionally distributed precursor sources. The presence of a southwest influence for SVOOA in NWR/PR suggests an additional contribution from relatively fresher emissions nearer to the site compared to LVOOA, consistent with the idea that semi-volatile oxygenated aerosol can respond rapidly to local-to-regional precursor inputs and thermodynamic partitioning.

SFCOA exhibits one of the strongest northwest directional signatures, with high concentrations in NWR (25-30 μg m^{-3}) at moderate wind speeds and PR enhancements extending into high wind-speed bins (60-80+ percentile). CWT identifies SFCOA hotspots (12-16 μg m^{-3}) concentrated in Punjab and western Haryana, consistent with widespread residential solid-fuel use and small-scale combustion emissions across rural/agricultural districts. These transport signatures are consistent with trajectory-based estimates indicating that northwesterly winds can deliver stubble-burning aerosol to the Delhi region within ~15-51 hours depending on source distance (185-420 km) (Bikkina et al., 2019; Cusworth et al., 2018). BBOA also shows northwest influence, but with a somewhat broader spatial distribution, consistent with contributions from both intense agricultural burning and more distributed residential biomass burning. The coherence of SFCOA and BBOA regional signatures reinforces that what is often labeled as Delhi haze is, in substantial part, the manifestation of a broader IGP combustion plume that is already heavily polluted and chemically evolved before reaching the city (Sharma et al., 2020).

The BC apportionment reinforces this regional narrative. eBC_{bb} shows strong northwest directionality in NWR (15-20 µg m^{-3}), increasing concentrations under moderate-to-high wind speeds in PR, and distinct CWT hotspots (7-10 µg m^{-3}) co-located with SFCOA and BBOA source regions. The tri-method agreement (NWR direction, PR wind-speed dependence, and CWT geographic localization) provides robust evidence that biomass burning dominates BC at Sonipat during this period. In contrast, eBC_{ff} is comparatively small (5-10 µg m^{-3}), exhibits a centre-weighted NWR pattern, is associated mainly with lower wind-speed bins in PR, and shows weak/limited spatial structure in CWT (<3 µg m^{-3}). This indicates predominately local fossil-fuel influence with minimal regional transport signatures. The strong contrast between eBC_{bb} and eBC_{ff} at Sonipat is consistent with its role as an intermediate receptor site, where transported biomass-burning plumes are intercepted before dilution by Delhi's urban fossil fuel emissions, and it suggests that reductions in regional biomass burning could produce immediate downwind benefits by lowering the incoming BC burden that contributes to both exposure and aerosol absorption.

HOA remains low (5-10 µg m^{-3}) and displays center-weighted NWR behavior, broad directional spread in PR at low wind speeds, and minimal spatial structure in CWT (<3 µg m^{-3}), indicating that HOA is dominated by local traffic with negligible long-range transport. This differs from many Delhi urban studies where HOA is higher and transport contributions to $PM_{2.5}$ can be substantial (Pant et al., 2015). The weak regional signature in HOA at Sonipat provides an important contrast: the regional plume arriving at Sonipat is strongly biomass/solid-fuel dominated, and traffic-related emissions become more important only after mixing within the Delhi urban environment. This upwind–downwind contrast supports the interpretation that policies targeting only urban traffic will not substantially reduce the regional carbonaceous plume that sets the baseline for Delhi-NCR haze, whereas coordinated actions addressing agricultural burning and solid-fuel combustion across the corridor are likely to be more effective for reducing both upwind and downwind exposure.

https://doi.org/10.5194/egusphere-2026-1428
Preprint. Discussion started: 15 April 2026

Overall, the integrated NWR-PR-CWT evidence indicates that the Sonipat site experienced overwhelming regional influence during the post-monsoon period, with Punjab-Haryana agricultural regions consistently identified as dominant source areas for aged, oxygenated OA, solid-fuel combustion OA, and biomass-derived BC. Secondary OA (LVOOA + SVOOA) frequently reached combined levels approaching 80-100 µg m^{-3} during intense haze, and biomass-related combustion factors (SFCOA, BBOA, eBC_{bb}) exhibited coherent transport signatures and geographically consistent hotspots. At the same time, HOA remained low and locally influenced. These results establish Sonipat as a sensitive receptor for transboundary biomass-burning emissions and their processed products before they mix with Delhi's urban emissions, underscoring that effective mitigation of post-monsoon haze across Delhi-NCR requires addressing regional combustion sources along the broader IGP transport corridor and aligning short-term actions with meteorological forecasts that identify high risk stagnation periods.

4. Summary and Conclusions

This study presents the first comprehensive, high-time-resolution source apportionment of carbonaceous $PM_{2.5}$ at Sonipat, an upwind receptor site located ~40 km northwest of Delhi along the principal post-monsoon transport corridor linking the Punjab-Haryana agricultural burning regions with the Delh-NCR, providing detailed insights into the chemical evolution and source dynamics that drive severe haze episodes across the Indo-Gangetic Plain. By integrating ToF-ACSM measurements, Aethalometer-based black carbon apportionment, Positive Matrix Factorization (PMF), and trajectory- and wind-based diagnostics, we quantified the relative contributions of primary combustion emissions, secondary processing, and meteorological controls in shaping haze evolution prior to mixing with urban emissions.

Two major haze episodes during 25 October–15 November 2023 were characterized by composition-based $PM_{2.5}$ exceeding 300 µg m^{-3}. Organic aerosol (OA) dominated the submicron mass, accounting for ~65% of NR-$PM_{2.5}$, with daily mean OA peaking near 140 µg m^{-3} during the first haze episode. PMF resolved five factors, namely, hydrocarbon-like OA (HOA), biomass-burning OA (BBOA), solid-fuel combustion OA (SFCOA), and two oxygenated components (SVOOA and LVOOA). Secondary organic aerosol (SVOOA + LVOOA) constituted ~57-60% of OA mass across the campaign, with LVOOA alone representing the largest fraction (mean 25 µg m^{-3}) and reaching 42.8 µg m^{-3} during the most intense haze period, indicating substantial regional aging and multi-day accumulation. Primary combustion related components also increased sharply during haze, with SFCOA and BBOA showing strong enhancements relative to non-haze conditions. Black carbon apportionment revealed a pronounced biomass-burning dominance, with biomass-derived BC (eBC$_{bb}$) contributing ~78% of total eBC (mean 10.9 µg m^{-3}), substantially exceeding fossil-fuel BC (3.1 µg m^{-3}). During the peak haze episode, eBC$_{bb}$ reached 14.2 µg m^{-3}. This reversed BC partitioning relative to urban Delhi confirms that the upwind plume intercepted at Sonipat is strongly influenced by regional biomass and solid-fuel combustion rather than traffic-dominated emissions.

The transition from non-haze to haze conditions reflects amplification of a persistently elevated regional carbonaceous background. Even during non-haze periods, oxidized OA (LVOOA ~11-13 µg m^{-3}) remained substantial, indicating sustained regional processing across the Indo-Gangetic Plain. During haze, sharp increases in SFCOA and BBOA were superimposed on this aged baseline, driving extreme mass loadings. Notably, secondary components (SOA plus secondary inorganics) continued to account for ~56-60% of C-PM$_{2.5}$ even under extreme pollution (>200 µg m^{-3}), demonstrating that haze severity arises from the combined effects of direct combustion emissions, abundant precursors, and meteorologically driven secondary growth. Distinct differences between haze episodes further suggest that prolonged stagnation favors accumulation of highly aged LVOOA, whereas shorter duration emission pulses (e.g., Diwali) are associated with comparatively fresher oxygenated fractions.

Independent trajectory and wind-regression analyses consistently identified northwestern transport from Punjab-Haryana agricultural districts as the dominant source influence during polluted periods. LVOOA, SVOOA, SFCOA, and eBC$_{bb}$ exhibited coherent northwest signatures and concentration-weighted trajectory hotspots aligned with agricultural burning regions, whereas HOA remained low and largely local in origin. These findings establish Sonipat as a regional receptor site intercepting a combustion-dominated plume prior to mixing with Delhi's urban emissions and demonstrate that extreme carbonaceous loading can develop outside the urban core.

The results of this study show that post-monsoon haze over the Delhi-NCR is strongly shaped by regionally transported biomass and solid-fuel combustion emissions and by sustained secondary organic aerosol formation under stagnant meteorological conditions. A substantial fraction of the pollution burden affecting Delhi is therefore already pre-formed before entering the city. Effective mitigation of severe haze requires coordinated, airshed-scale emission reductions targeting agricultural residue burning, rural solid-fuel combustion, and regional precursor gases. Strategies focused solely on urban traffic or primary emissions are unlikely to sufficiently reduce peak pollution if secondary formation remains dominant. Integrated regional controls, aligned with meteorological forecasts of stagnation, are essential for achieving durable reductions in $PM_{2.5}$ exposure across the broader Indo-Gangetic Plain and the Delhi-NCR.

Acknowledgements

Authors are grateful to the Head, Centre for Atmospheric Sciences and Director, IIT Delhi, for necessary support. VS and JR thanks the IITD for providing research fellowship. We gratefully acknowledge the use of data products from NOAA Hysplit Model. We also thank Shahzad Gani for his contribution to the observatory.

Data availability

- The observational datasets used in this study and meteorological parameters from the automatic weather station (AWS) installed at the Sonipat site (Rathore et al., 2025) , are available at https://doi.org/10.5281/zenodo.15902605.
- The fire counts data can be accessed from https://firms.modaps.eosdis.nasa.gov/.
- ZeFir is used for wind and trajectory-based analysis(https://sites.google.com/site/zefirproject).
- All plots in this study were generated using Python (https://www.anaconda.com/download).

https://doi.org/10.5194/egusphere-2026-1428
Preprint. Discussion started: 15 April 2026

Author Contributions:

Conceptualization: VS, DG, SD

Data curation: VS, JR

Investigation, Methodology: VS, DG,SD,JR

Software, Visualization: VS

Writing – original draft: VS

Writing – review & editing: DG, JR, SD, RKK, LS

Resources- DG, SG, SD, RKK, LS

Competing Interest

The authors declare no conflicts of interest relevant to this study.

5. References

Bhandari, S., Gani, S., Patel, K., Wang, D.S., Soni, P., Arub, Z., Habib, G., Apte, J.S., Hildebrandt Ruiz, L., 2020. Sources and atmospheric dynamics of organic aerosol in New Delhi, India: insights from receptor modeling. Atmos. Chem. Phys. 20, 735–752. https://doi.org/10.5194/acp-20-735-2020

Bhowmik, H.S., Tripathi, S.N., Sahu, R., Shukla, A.K., Lalchandani, V., Talukdar, S., Tripathi, N., Sahu, L., 2022. Insights into the Regional Transport and Local Formation of Secondary Organic Aerosol in Delhi, India. Aerosol Air Qual. Res. 22, 220113. https://doi.org/10.4209/aaqr.220113

Bikkina, S., Andersson, A., Kirillova, E.N., Holmstrand, H., Tiwari, S., Srivastava, A.K., Bisht, D.S., Gustafsson, Ö., 2019. Air quality in megacity Delhi affected by countryside biomass burning. Nat Sustain 2, 200–205. https://doi.org/10.1038/s41893-019-0219-0

Biswal, A., Singh, V., Malik, L., Tiwari, G., Ravindra, K., Mor, S., 2023. Spatially resolved hourly traffic emission over megacity Delhi using advanced traffic flow data. Earth Syst. Sci. Data 15, 661–680. https://doi.org/10.5194/essd-15-661-2023

Canagaratna, M.R., Jimenez, J.L., Kroll, J.H., Chen, Q., Kessler, S.H., Massoli, P., Hildebrandt Ruiz, L., Fortner, E., Williams, L.R., Wilson, K.R., Surratt, J.D., Donahue, N.M., Jayne, J.T., Worsnop, D.R., 2015. Elemental ratio measurements of organic compounds using aerosol mass spectrometry: characterization, improved calibration, and implications. Atmos. Chem. Phys. 15, 253–272. https://doi.org/10.5194/acp-15-253-2015

Canonaco, F., Crippa, M., Slowik, J.G., Baltensperger, U., Prévôt, A.S.H., 2013. SoFi, an IGOR-based interface for the efficient use of the generalized multilinear engine (ME-2) for the source apportionment: ME-2 application to aerosol mass spectrometer data. Atmos. Meas. Tech. 6, 3649–3661. https://doi.org/10.5194/amt-6-3649-2013

Canonaco, F., Tobler, A., Chen, G., Sosedova, Y., Slowik, J.G., Bozzetti, C., Daellenbach, K.R., El Haddad, I., Crippa, M., Huang, R.-J., Furger, M., Baltensperger, U., Prévôt, A.S.H., 2021. A new method for long-term source apportionment with time-dependent factor profiles and uncertainty assessment using SoFi Pro: application to 1 year of organic aerosol data. Atmos. Meas. Tech. 14, 923–943. https://doi.org/10.5194/amt-14-923-2021

Cash, J.M., Di Marco, C., Langford, B., Heal, M.R., Mandal, T.K., Sharma, S.K., Gurjar, B.R., Nemitz, E., 2023. Response of organic aerosol to Delhi's pollution control measures over the period 2011–2018. Atmospheric Environment 315, 120123. https://doi.org/10.1016/j.atmosenv.2023.120123

Cash, J.M., Langford, B., Di Marco, C., Mullinger, N.J., Allan, J., Reyes-Villegas, E., Joshi, R., Heal, M.R., Acton, W.J.F., Hewitt, C.N., Misztal, P.K., Drysdale, W., Mandal, T.K.,

https://doi.org/10.5194/egusphere-2026-1428
Preprint. Discussion started: 15 April 2026

Shivani, Gadi, R., Gurjar, B.R., Nemitz, E., 2021. Seasonal analysis of submicron aerosol in Old Delhi using high-resolution aerosol mass spectrometry: chemical characterisation, source apportionment and new marker identification. Atmos. Chem. Phys. 21, 10133–10158. https://doi.org/10.5194/acp-21-10133-2021

Crippa, M., El Haddad, I., Slowik, J.G., DeCarlo, P.F., Mohr, C., Heringa, M.F., Chirico, R., Marchand, N., Sciare, J., Baltensperger, U., Prévôt, A.S.H., 2013. Identification of marine and continental aerosol sources in Paris using high resolution aerosol mass spectrometry. JGR Atmospheres 118, 1950–1963. https://doi.org/10.1002/jgrd.50151

Cusworth, D.H., Mickley, L.J., Sulprizio, M.P., Liu, T., Marlier, M.E., DeFries, R.S., Guttikunda, S.K., Gupta, P., 2018. Quantifying the influence of agricultural fires in northwest India on urban air pollution in Delhi, India. Environ. Res. Lett. 13, 044018. https://doi.org/10.1088/1748-9326/aab303

Dey, S., Di Girolamo, L., 2010. A climatology of aerosol optical and microphysical properties over the Indian subcontinent from 9 years (2000–2008) of Multiangle Imaging Spectroradiometer (MISR) data. J. Geophys. Res. 115, 2009JD013395. https://doi.org/10.1029/2009JD013395

Dumka, U.C., Kaskaoutis, D.G., Tiwari, S., Safai, P.D., Attri, S.D., Soni, V.K., Singh, N., Mihalopoulos, N., 2018. Assessment of biomass burning and fossil fuel contribution to black carbon concentrations in Delhi during winter. Atmospheric Environment 194, 93–109. https://doi.org/10.1016/j.atmosenv.2018.09.033

Fröhlich, R., Cubison, M.J., Slowik, J.G., Bukowiecki, N., Prévôt, A.S.H., Baltensperger, U., Schneider, J., Kimmel, J.R., Gonin, M., Rohner, U., Worsnop, D.R., Jayne, J.T., 2013. The ToF-ACSM: a portable aerosol chemical speciation monitor with TOFMS detection. Atmos. Meas. Tech. 6, 3225–3241. https://doi.org/10.5194/amt-6-3225-2013

Ganguly, D., Ginoux, P., Ramaswamy, V., Winker, D.M., Holben, B.N., Tripathi, S.N., 2009. Retrieving the composition and concentration of aerosols over the Indo-Gangetic basin using CALIOP and AERONET data. Geophysical Research Letters 36, 2009GL038315. https://doi.org/10.1029/2009GL038315

Gani, S., Bhandari, S., Patel, K., Seraj, S., Soni, P., Arub, Z., Habib, G., Hildebrandt Ruiz, L., Apte, J.S., 2020. Particle number concentrations and size distribution in a polluted megacity: the Delhi Aerosol Supersite study. Atmos. Chem. Phys. 20, 8533–8549. https://doi.org/10.5194/acp-20-8533-2020

Gani, S., Bhandari, S., Seraj, S., Wang, D.S., Patel, K., Soni, P., Arub, Z., Habib, G., Hildebrandt Ruiz, L., Apte, J.S., 2019. Submicron aerosol composition in the world's most polluted megacity: the Delhi Aerosol Supersite study. Atmos. Chem. Phys. 19, 6843–6859. https://doi.org/10.5194/acp-19-6843-2019

Ghude, S.D., Chate, D.M., Jena, C., Beig, G., Kumar, R., Barth, M.C., Pfister, G.G., Fadnavis, S., Pithani, P., 2016. Premature mortality in India due to $PM_{2.5}$ and ozone exposure. Geophysical Research Letters 43, 4650–4658. https://doi.org/10.1002/2016GL068949

Ghude, S.D., Govardhan, G., Kumar, R., Yadav, P.P., Jat, R., Debnath, S., Kalita, G., Jena, C., Ingle, S., Gunwani, P., Pawar, P.V., Ambulkar, R., Kumar, S., Kulkarni, S., Kulkarni, A., Khare, M., Kaginalkar, A., Soni, V.K., Nigam, N., Ray, K., Atri, S.D., Nanjundiah, R., Rajeevan, M., 2024. Air Quality Warning and Integrated Decision Support System for Emissions (AIRWISE): Enhancing Air Quality Management in Megacities. Bulletin of the American Meteorological Society 105, E2525–E2550. https://doi.org/10.1175/BAMS-D-23-0181.1

Goel, V., Hazarika, N., Kumar, M., Singh, V., 2021. Source apportionment of black carbon over Delhi: A case study of extreme biomass burning events and Diwali festival. Urban Climate 39, 100926. https://doi.org/10.1016/j.uclim.2021.100926

Goel, V., Tripathi, N., Gupta, M., Sahu, L.K., Singh, V., Kumar, M., 2024. Study of secondary organic aerosol formation and aging using ambient air in an oxidation flow reactor during

https://doi.org/10.5194/egusphere-2026-1428
Preprint. Discussion started: 15 April 2026

high pollution events over Delhi. Environmental Research 251, 118542. https://doi.org/10.1016/j.envres.2024.118542

Gunthe, S.S., Liu, P., Panda, U., Raj, S.S., Sharma, A., Darbyshire, E., Reyes-Villegas, E., Allan, J., Chen, Y., Wang, X., Song, S., Pöhlker, M.L., Shi, L., Wang, Y., Kommula, S.M., Liu, T., Ravikrishna, R., McFiggans, G., Mickley, L.J., Martin, S.T., Pöschl, U., Andreae, M.O., Coe, H., 2021. Enhanced aerosol particle growth sustained by high continental chlorine emission in India. Nat. Geosci. 14, 77–84. https://doi.org/10.1038/s41561-020-00677-x

Guo, J., Zhou, S., Cai, M., Zhao, J., Song, W., Zhao, W., Hu, W., Sun, Y., He, Y., Yang, C., Xu, X., Zhang, Z., Cheng, P., Fan, Q., Hang, J., Fan, S., Wang, Xinming, Wang, Xuemei, 2020. Characterization of submicron particles by time-of-flight aerosol chemical speciation monitor (ToF-ACSM) during wintertime: aerosol composition, sources, and chemical processes in Guangzhou, China. Atmos. Chem. Phys. 20, 7595–7615. https://doi.org/10.5194/acp-20-7595-2020

Gupta, T., Rajeev, P., Rajput, R., 2022. Emerging Major Role of Organic Aerosols in Explaining the Occurrence, Frequency, and Magnitude of Haze and Fog Episodes during Wintertime in the Indo Gangetic Plain. ACS Omega 7, 1575–1584. https://doi.org/10.1021/acsomega.1c05467

Guttikunda, S.K., Calori, G., 2013. A GIS based emissions inventory at 1 km × 1 km spatial resolution for air pollution analysis in Delhi, India. Atmospheric Environment 67, 101–111. https://doi.org/10.1016/j.atmosenv.2012.10.040

Harrison, R.M., Beddows, D.C.S., Jones, A.M., Calvo, A., Alves, C., Pio, C., 2013. An evaluation of some issues regarding the use of aethalometers to measure woodsmoke concentrations. Atmospheric Environment 80, 540–548. https://doi.org/10.1016/j.atmosenv.2013.08.026

Haslett, S.L., Bell, D.M., Kumar, V., Slowik, J.G., Wang, D.S., Mishra, S., Rastogi, N., Singh, A., Ganguly, D., Thornton, J., Zheng, F., Li, Y., Nie, W., Liu, Y., Ma, W., Yan, C., Kulmala, M., Daellenbach, K.R., Hadden, D., Baltensperger, U., Prevot, A.S.H., Tripathi, S.N., Mohr, C., 2023. Nighttime NO emissions strongly suppress chlorine and nitrate radical formation during the winter in Delhi. Atmos. Chem. Phys. 23, 9023–9036. https://doi.org/10.5194/acp-23-9023-2023

Henry, R., Norris, G.A., Vedantham, R., Turner, J.R., 2009. Source Region Identification Using Kernel Smoothing. Environ. Sci. Technol. 43, 4090–4097. https://doi.org/10.1021/es8011723

Hu, W., Day, D.A., Campuzano-Jost, P., Nault, B.A., Park, T., Lee, T., Croteau, P., Canagaratna, M.R., Jayne, J.T., Worsnop, D.R., Jimenez, J.L., 2018. Evaluation of the New Capture Vaporizer for Aerosol Mass Spectrometers (AMS): Elemental Composition and Source Apportionment of Organic Aerosols (OA). ACS Earth Space Chem. 2, 410–421. https://doi.org/10.1021/acsearthspacechem.8b00002

Jain, S., Sharma, S.K., Srivastava, M.K., Chaterjee, A., Singh, R.K., Saxena, M., Mandal, T.K., 2019. Source Apportionment of PM10 Over Three Tropical Urban Atmospheres at Indo-Gangetic Plain of India: An Approach Using Different Receptor Models. Arch Environ Contam Toxicol 76, 114–128. https://doi.org/10.1007/s00244-018-0572-4

Jethva, H., Torres, O., Field, R.D., Lyapustin, A., Gautam, R., Kayetha, V., 2019. Connecting Crop Productivity, Residue Fires, and Air Quality over Northern India. Sci Rep 9, 16594. https://doi.org/10.1038/s41598-019-52799-x

Kumar, R.R., Soni, V.K., Jain, M.K., 2020. Evaluation of spatial and temporal heterogeneity of black carbon aerosol mass concentration over India using three year measurements from IMD BC observation network. Science of The Total Environment 723, 138060. https://doi.org/10.1016/j.scitotenv.2020.138060

Lakra, A., Shukla, A.K., Bhowmik, H.S., Yadav, A.K., Jain, V., Murari, V., Gaddamidi, S., Lalchandani, V., Tripathi, S.N., 2024. Comparative analysis of winter composite-PM2.5 in Central Indo Gangetic Plain cities: Combined organic and inorganic source apportionment and characterization, with a focus on the photochemical age effect on secondary organic aerosol formation. Atmospheric Environment 338, 120827. https://doi.org/10.1016/j.atmosenv.2024.120827

Lalchandani, V., Kumar, V., Tobler, A., M. Thamban, N., Mishra, S., Slowik, J.G., Bhattu, D., Rai, P., Satish, R., Ganguly, D., Tiwari, Suresh, Rastogi, N., Tiwari, Shashi, Močnik, G., Prévôt, A.S.H., Tripathi, S.N., 2021. Real-time characterization and source apportionment of fine particulate matter in the Delhi megacity area during late winter. Science of The Total Environment 770, 145324. https://doi.org/10.1016/j.scitotenv.2021.145324

Lalchandani, V., Srivastava, D., Dave, J., Mishra, S., Tripathi, N., Shukla, A.K., Sahu, R., Thamban, N.M., Gaddamidi, S., Dixit, K., Ganguly, D., Tiwari, S., Srivastava, A.K., Sahu, L., Rastogi, N., Gargava, P., Tripathi, S.N., 2022. Effect of Biomass Burning on $PM_{2.5}$ Composition and Secondary Aerosol Formation During Post-Monsoon and Winter Haze Episodes in Delhi. JGR Atmospheres 127, e2021JD035232. https://doi.org/10.1029/2021JD035232

Lanz, V.A., Alfarra, M.R., Baltensperger, U., Buchmann, B., Hueglin, C., Prévôt, A.S.H., 2007. Source apportionment of submicron organic aerosols at an urban site by factor analytical modelling of aerosol mass spectra. Atmos. Chem. Phys. 7, 1503–1522. https://doi.org/10.5194/acp-7-1503-2007

Mathai, S., Ijaz, A., Gautam, T., Cheng, Z., Lata, N.N., Bhotika, H., Tseng, D., Chu, R.K., Mazzoleni, L., Mazzoleni, C., China, S., 2026. Haze processing of atmospheric particles during wintertime in the Indo-Gangetic Plains. Environ. Sci.: Atmos. 6, 139–151. https://doi.org/10.1039/D5EA00150A

https://doi.org/10.5194/egusphere-2026-1428
Preprint. Discussion started: 15 April 2026

Nair, V.S., Moorthy, K.K., Alappattu, D.P., Kunhikrishnan, P.K., George, S., Nair, P.R., Babu, S.S., Abish, B., Satheesh, S.K., Tripathi, S.N., Niranjan, K., Madhavan, B.L., Srikant, V., Dutt, C.B.S., Badarinath, K.V.S., Reddy, R.R., 2007. Wintertime aerosol characteristics over the Indo-Gangetic Plain (IGP): Impacts of local boundary layer processes and long-range transport. J. Geophys. Res. 112, 2006JD008099. https://doi.org/10.1029/2006JD008099

Nault, B.A., Croteau, P., Jayne, J., Williams, A., Williams, L., Worsnop, D., Katz, E.F., DeCarlo, P.F., Canagaratna, M., 2023. Laboratory evaluation of organic aerosol relative ionization efficiencies in the aerodyne aerosol mass spectrometer and aerosol chemical speciation monitor. Aerosol Science and Technology 57, 981–997. https://doi.org/10.1080/02786826.2023.2223249

Ng, N.L., Canagaratna, M.R., Jimenez, J.L., Zhang, Q., Ulbrich, I.M., Worsnop, D.R., 2011. Real-Time Methods for Estimating Organic Component Mass Concentrations from Aerosol Mass Spectrometer Data. Environ. Sci. Technol. 45, 910–916. https://doi.org/10.1021/es102951k

Ng, N.L., Canagaratna, M.R., Zhang, Q., Jimenez, J.L., Tian, J., Ulbrich, I.M., Kroll, J.H., Docherty, K.S., Chhabra, P.S., Bahreini, R., Murphy, S.M., Seinfeld, J.H., Hildebrandt, L., Donahue, N.M., DeCarlo, P.F., Lanz, V.A., Prévôt, A.S.H., Dinar, E., Rudich, Y., Worsnop, D.R., 2010. Organic aerosol components observed in Northern Hemispheric datasets from Aerosol Mass Spectrometry. Atmos. Chem. Phys. 10, 4625–4641. https://doi.org/10.5194/acp-10-4625-2010

Paatero, P., Tapper, U., 1994. Positive matrix factorization: A non-negative factor model with optimal utilization of error estimates of data values. Environmetrics 5, 111–126. https://doi.org/10.1002/env.3170050203

Panda, U., Dey, S., Sharma, A., Singh, A., Reyes-Villegas, E., Darbyshire, E., Carbone, S., Das, T., Allan, J., McFiggans, G., Ravikrishna, R., Coe, H., Liu, P., Gunthe, S.S., 2025.

Exploring the chemical composition and processes of submicron aerosols in Delhi using aerosol chemical speciation monitor driven factor analysis. Sci Rep 15, 14383. https://doi.org/10.1038/s41598-025-99245-9

Pandey, A., Brauer, M., Cropper, M.L., Balakrishnan, K., Mathur, P., Dey, Sagnik, Turkgulu, B., Kumar, G.A., Khare, M., Beig, G., Gupta, T., Krishnankutty, R.P., Causey, K., Cohen, A.J., Bhargava, S., Aggarwal, A.N., Agrawal, A., Awasthi, S., Bennitt, F., Bhagwat, S., Bhanumati, P., Burkart, K., Chakma, J.K., Chiles, T.C., Chowdhury, S., Christopher, D.J., Dey, Subhojit, Fisher, S., Fraumeni, B., Fuller, R., Ghoshal, A.G., Golechha, M.J., Gupta, P.C., Gupta, Rachita, Gupta, Rajeev, Gupta, S., Guttikunda, S., Hanrahan, D., Harikrishnan, S., Jeemon, P., Joshi, T.K., Kant, R., Kant, S., Kaur, T., Koul, P.A., Kumar, Praveen, Kumar, R., Larson, S.L., Lodha, R., Madhipatla, K.K., Mahesh, P.A., Malhotra, R., Managi, S., Martin, K., Mathai, M., Mathew, J.L., Mehrotra, R., Mohan, B.V.M., Mohan, V., Mukhopadhyay, S., Mutreja, P., Naik, N., Nair, S., Pandian, J.D., Pant, P., Perianayagam, A., Prabhakaran, D., Prabhakaran, P., Rath, G.K., Ravi, S., Roy, A., Sabde, Y.D., Salvi, S., Sambandam, S., Sharma, B., Sharma, M., Sharma, S., Sharma, R.S., Shrivastava, A., Singh, S., Singh, V., Smith, R., Stanaway, J.D., Taghian, G., Tandon, N., Thakur, J.S., Thomas, N.J., Toteja, G.S., Varghese, C.M., Venkataraman, C., Venugopal, K.N., Walker, K.D., Watson, A.Y., Wozniak, S., Xavier, D., Yadama, G.N., Yadav, G., Shukla, D.K., Bekedam, H.J., Reddy, K.S., Guleria, R., Vos, T., Lim, S.S., Dandona, R., Kumar, S., Kumar, Pushpam, Landrigan, P.J., Dandona, L., 2021. Health and economic impact of air pollution in the states of India: the Global Burden of Disease Study 2019. The Lancet Planetary Health 5, e25–e38. https://doi.org/10.1016/S2542-5196(20)30298-9

Pant, P., Guttikunda, S.K., Peltier, R.E., 2016. Exposure to particulate matter in India: A synthesis of findings and future directions. Environmental Research 147, 480–496. https://doi.org/10.1016/j.envres.2016.03.011

Pant, P., Shukla, A., Kohl, S.D., Chow, J.C., Watson, J.G., Harrison, R.M., 2015. Characterization of ambient PM2.5 at a pollution hotspot in New Delhi, India and inference of sources. Atmospheric Environment 109, 178–189. https://doi.org/10.1016/j.atmosenv.2015.02.074

Petit, J.-E., Favez, O., Albinet, A., Canonaco, F., 2017. A user-friendly tool for comprehensive evaluation of the geographical origins of atmospheric pollution: Wind and trajectory analyses. Environmental Modelling & Software 88, 183–187. https://doi.org/10.1016/j.envsoft.2016.11.022

Petzold, A., Ogren, J.A., Fiebig, M., Laj, P., Li, S.-M., Baltensperger, U., Holzer-Popp, T., Kinne, S., Pappalardo, G., Sugimoto, N., Wehrli, C., Wiedensohler, A., Zhang, X.-Y., 2013. Recommendations for reporting “black carbon” measurements. Atmos. Chem. Phys. 13, 8365–8379. https://doi.org/10.5194/acp-13-8365-2013

Rathore, J., Ganguly, D., Singh, V., Gupta, M., Vazhathara, V.J., Biswal, A., Kunchala, R.K., Patra, P.K., Sahu, L.K., Gani, S., Dey, S., 2025. Characteristics of Haze Pollution Events During Biomass Burning Period at an Upwind Site of Delhi. JGR Atmospheres 130, e2024JD042347. https://doi.org/10.1029/2024JD042347

Reyes-Villegas, E., Panda, U., Darbyshire, E., Cash, J.M., Joshi, R., Langford, B., Di Marco, C.F., Mullinger, N.J., Alam, M.S., Crilley, L.R., Rooney, D.J., Acton, W.J.F., Drysdale, W., Nemitz, E., Flynn, M., Voliotis, A., McFiggans, G., Coe, H., Lee, J., Hewitt, C.N., Heal, M.R., Gunthe, S.S., Mandal, T.K., Gurjar, B.R., Shivani, Gadi, R., Singh, S., Soni, V., Allan, J.D., 2021. PM_1 composition and source apportionment at two sites in Delhi, India, across multiple seasons. Atmos. Chem. Phys. 21, 11655–11667. https://doi.org/10.5194/acp-21-11655-2021

Sahu, L.K., Kondo, Y., Moteki, N., Takegawa, N., Zhao, Y., Cubison, M.J., Jimenez, J.L., Vay, S., Diskin, G.S., Wisthaler, A., Mikoviny, T., Huey, L.G., Weinheimer, A.J., Knapp, D.J., 2012. Emission characteristics of black carbon in anthropogenic and biomass burning plumes over California during ARCTAS-CARB 2008. J. Geophys. Res. 117, 2011JD017401. https://doi.org/10.1029/2011JD017401

Sandradewi, J., Prévôt, A.S.H., Szidat, S., Perron, N., Alfarra, M.R., Lanz, V.A., Weingartner, E., Baltensperger, U., 2008. Using Aerosol Light Absorption Measurements for the Quantitative Determination of Wood Burning and Traffic Emission Contributions to Particulate Matter. Environ. Sci. Technol. 42, 3316–3323. https://doi.org/10.1021/es702253m

Sarkar, S., Singh, R.P., Chauhan, A., 2018. Crop Residue Burning in Northern India: Increasing Threat to Greater India. JGR Atmospheres 123, 6920–6934. https://doi.org/10.1029/2018JD028428

Satish, R., Shamjad, P., Thamban, N., Tripathi, S., Rastogi, N., 2017. Temporal Characteristics of Brown Carbon over the Central Indo-Gangetic Plain. Environ. Sci. Technol. 51, 6765–6772. https://doi.org/10.1021/acs.est.7b00734

Segura, S., Estellés, V., Titos, G., Lyamani, H., Utrillas, M.P., Zotter, P., Prévôt, A.S.H., Močnik, G., Alados-Arboledas, L., Martínez-Lozano, J.A., 2014. Determination and analysis of in situ spectral aerosol optical properties by a multi-instrumental approach. Atmos. Meas. Tech. 7, 2373–2387. https://doi.org/10.5194/amt-7-2373-2014

Sharma, S., Zhang, M., Anshika, Gao, J., Zhang, H., Kota, S.H., 2020. Effect of restricted emissions during COVID-19 on air quality in India. Science of The Total Environment 728, 138878. https://doi.org/10.1016/j.scitotenv.2020.138878

Sharma, S.K., Mandal, T.K., Jain, S., Saraswati, Sharma, A., Saxena, M., 2016. Source Apportionment of PM2.5 in Delhi, India Using PMF Model. Bull Environ Contam Toxicol 97, 286–293. https://doi.org/10.1007/s00128-016-1836-1

Shiraiwa, M., Kondo, Y., Moteki, N., Takegawa, N., Sahu, L.K., Takami, A., Hatakeyama, S., Yonemura, S., Blake, D.R., 2008. Radiative impact of mixing state of black carbon aerosol in Asian outflow. J. Geophys. Res. 113, 2008JD010546. https://doi.org/10.1029/2008JD010546

Shukla, A.K., Lalchandani, V., Bhattu, D., Dave, J.S., Rai, P., Thamban, N.M., Mishra, S., Gaddamidi, S., Tripathi, N., Vats, P., Rastogi, N., Sahu, L., Ganguly, D., Kumar, M., Singh, V., Gargava, P., Tripathi, S.N., 2021. Real-time quantification and source apportionment of fine particulate matter including organics and elements in Delhi during summertime. Atmospheric Environment 261, 118598. https://doi.org/10.1016/j.atmosenv.2021.118598

Shukla, A.K., Tripathi, S.N., Canonaco, F., Lalchandani, V., Sahu, R., Srivastava, D., Dave, J., Thamban, N.M., Gaddamidi, S., Sahu, L., Kumar, M., Singh, V., Rastogi, N., 2023. Spatio-temporal variation of C-PM2.5 (composition based PM2.5) sources using PMF*PMF (double-PMF) and single-combined PMF technique on real-time non-refractory, BC and elemental measurements during post-monsoon and winter at two sites in Delhi, India. Atmospheric Environment 293, 119456. https://doi.org/10.1016/j.atmosenv.2022.119456

Shukla, A.K., Tripathi, S.N., Talukdar, S., Murari, V., Gaddamidi, S., Manousakas, M.-I., Lalchandani, V., Dixit, K., Ruge, V.M., Khare, P., Kumar, M., Singh, V., Rastogi, N., Tiwari, S., Srivastava, A.K., Ganguly, D., Daellenbach, K.R., Prévôt, A.S.H., 2025. Measurement report: Sources and meteorology influencing highly time-resolved $PM_{2.5}$ trace elements at three urban sites in the extremely polluted Indo-Gangetic Plain in India. Atmos. Chem. Phys. 25, 3765–3784. https://doi.org/10.5194/acp-25-3765-2025

Singh, T., Matsumi, Y., Nakayama, T., Hayashida, S., Patra, P.K., Yasutomi, N., Kajino, M., Yamaji, K., Khatri, P., Takigawa, M., Araki, H., Kurogi, Y., Kuji, M., Muramatsu, K., Imasu, R., Ananda, A., Arbain, A.A., Ravindra, K., Bhardwaj, S., Kumar, S., Mor, Sahil, Dhaka, S.K., Dimri, A.P., Sharma, A., Singh, N., Bhatti, M.S., Yadav, R., Vatta, K., Mor, Suman, 2023. Very high particulate pollution over northwest India captured by a highdensity in situ sensor network. Sci Rep 13, 13201. https://doi.org/10.1038/s41598-023-39471-1

Singh, V., Singh, S., Biswal, A., 2021. Exceedances and trends of particulate matter (PM2.5) in five Indian megacities. Science of The Total Environment 750, 141461. https://doi.org/10.1016/j.scitotenv.2020.141461

Stein, A.F., Draxler, R.R., Rolph, G.D., Stunder, B.J.B., Cohen, M.D., Ngan, F., 2015. NOAA's HYSPLIT Atmospheric Transport and Dispersion Modeling System. Bulletin of the American Meteorological Society 96, 2059–2077. https://doi.org/10.1175/BAMS-D-14-00110.1

Thamban, N.M., Joshi, B., Tripathi, S.N., Sueper, D., Canagaratna, M.R., Moosakutty, S.P., Satish, R., Rastogi, N., 2019. Evolution of Aerosol Size and Composition in the Indo-Gangetic Plain: Size-Resolved Analysis of High-Resolution Aerosol Mass Spectra. ACS Earth Space Chem. 3, 823–832. https://doi.org/10.1021/acsearthspacechem.8b00207

Thamban, N.M., Lalchandani, V., Kumar, V., Mishra, S., Bhattu, D., Slowik, J.G., Prevot, A.S.H., Satish, R., Rastogi, N., Tripathi, S.N., 2021. Evolution of size and composition of fine particulate matter in the Delhi megacity during later winter. Atmospheric Environment 267, 118752. https://doi.org/10.1016/j.atmosenv.2021.118752

Titos, G., Del Águila, A., Cazorla, A., Lyamani, H., Casquero-Vera, J.A., Colombi, C., Cuccia, E., Gianelle, V., Močnik, G., Alastuey, A., Olmo, F.J., Alados-Arboledas, L., 2017. Spatial and temporal variability of carbonaceous aerosols: Assessing the impact of biomass burning in the urban environment. Science of The Total Environment 578, 613–625. https://doi.org/10.1016/j.scitotenv.2016.11.007

Tobler, A., Bhattu, D., Canonaco, F., Lalchandani, V., Shukla, A., Thamban, N.M., Mishra, S., Srivastava, A.K., Bisht, D.S., Tiwari, S., Singh, S., Močnik, G., Baltensperger, U., Tripathi, S.N., Slowik, J.G., Prévôt, A.S.H., 2020. Chemical characterization of PM2.5

and source apportionment of organic aerosol in New Delhi, India. Science of The Total Environment 745, 140924. https://doi.org/10.1016/j.scitotenv.2020.140924

Ulbrich, I.M., Canagaratna, M.R., Zhang, Q., Worsnop, D.R., Jimenez, J.L., 2009. Interpretation of organic components from Positive Matrix Factorization of aerosol mass spectrometric data. Atmos. Chem. Phys.

Yadav, S., Tripathi, S.N., Rupakheti, M., 2022. Current status of source apportionment of ambient aerosols in India. Atmospheric Environment 274, 118987. https://doi.org/10.1016/j.atmosenv.2022.118987

Zhang, Zirui, Zhu, W., Hu, M., Liu, K., Wang, H., Tang, R., Shen, R., Yu, Y., Tan, R., Song, K., Li, Y., Zhang, W., Zhang, Zhou, Xu, H., Shuai, S., Li, S., Chen, Y., Li, J., Wang, Y., Guo, S., 2021. Formation and evolution of secondary organic aerosols derived from urban-lifestyle sources: vehicle exhaust and cooking emissions. Atmos. Chem. Phys. 21, 15221–15237. https://doi.org/10.5194/acp-21-15221-2021

Zhao, J., Qiu, Y., Zhou, W., Xu, W., Wang, J., Zhang, Y., Li, L., Xie, C., Wang, Q., Du, W., Worsnop, D.R., Canagaratna, M.R., Zhou, L., Ge, X., Fu, P., Li, J., Wang, Z., Donahue, N.M., Sun, Y., 2019. Organic Aerosol Processing During Winter Severe Haze Episodes in Beijing. JGR Atmospheres 124, 10248–10263. https://doi.org/10.1029/2019JD030832

Zotter, P., Herich, H., Gysel, M., El-Haddad, I., Zhang, Y., Močnik, G., Hüglin, C., Baltensperger, U., Szidat, S., Prévôt, A.S.H., 2017. Evaluation of the absorption Ångström exponents for traffic and wood burning in the Aethalometer-based source apportionment using radiocarbon measurements of ambient aerosol. Atmos. Chem. Phys. 17, 4229–4249. https://doi.org/10.5194/acp-17-4229-2017